Charles University in Prague
Faculty of Mathematics and Physics

DIPLOMA THESIS

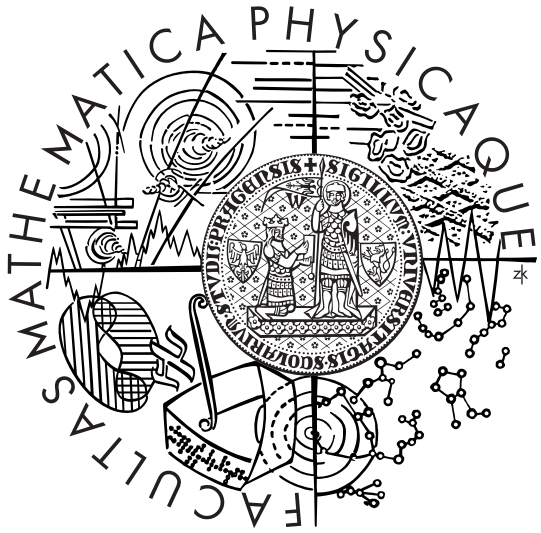

Jan Kratochvíl

Numerical simulations of flows of visco-elastic fluid-like materials, as asphalt in particular

Institute of Theoretical Physics

Supervisor: Doc. RNDr. Josef Málek, CSc.
Branch: Mathematical and computer modeling in science and technology

Prague 2007

Acknowledgment

I would like to thank Doc. RNDr. Josef Málek, CSc. for thoughtfully supervising my thesis, creating comfortable working environment and providing valuable information and corrections, RNDr. Ing. Jaroslav Hron, Ph.D. for numerous discussions and help with the software topics, Prof. K. R. Rajagopal for inspiring this thesis and Dr. J. Murali Krishnan for providing me with experimental data.

I would especially like to express my thanks to my parents for supporting me during the period of my studies.

This research was partly supported by the Czech Science Foundation through the project GACR 201/06/0352.

I declare that I wrote this thesis by myself and using only the cited sources. I agree with lending this thesis.

Prague, April 20, 2007 Jan Kratochvíl

Contents

Abstrakt

Název práce: *Numerické simulace deformací visko-elastických materiálů, zejména asfaltu*
Autor: *Jan Kratochvíl*
Katedra (ústav): *Ústav teoretické fyziky*
Vedoucí diplomové práce: *Doc. RNDr. Josef Málek, CSc., Matematický ústav UK*
e-mail vedoucího: *malek@karlin.mff.cuni.cz*
Abstrakt: Tato diplomová práce se zabývá numerickými simulacemi proudění viskoelastických tekutin. Nejprve jsou představeny dva modely pro tento typ tekutin, jednak klasický Oldroydův model a potom nový nelineární model, který je možné považovat za zobecnění modelu Oldroyd-B pro velké elastické deformace. Poté jsou provedeny výpočty proudění ve třech různých situacích. První z nich je relaxace napětí v rovinném proudění mezi rovnoběžnými deskami, což je příklad jednorozměrného problému. Druhou je rovinné proudění ve zúženém kanále, což je standardní dvourozměrný testovací příklad v oblasti viskoelastického proudění. Konečně třetí situací je relaxace napětí v osově symetrickém proudění ve válci, které bylo počítáno jednak jako jednorozměrný a jednak jako dvourozměrný problém. V případech, kdy je to možné, jsou výpočty provedeny analyticky, v ostatních případech numericky metodou konečných prvků s využitím programu Comsol Multiphysics 3.3. K válcové geometrii jsou dostupná experimentální data týkající se relaxace napětí v asfaltu. Tato data jsou v závěru práce nafitována pomocí obou uvažovaných modelů.
Klíčová slova: *viskoelastická tekutina, asfalt, metoda konečných prvků*

Abstract

Title: *Numerical simulations of flows of visco-elastic fluid-like materials, as asphalt in particular*
Author: *Jan Kratochvíl*
Department: *Institute of Theoretical Physics*
Supervisor: *Doc. RNDr. Josef Málek, CSc., Mathematical Institute of Charles University*
Supervisor's e-mail address: *malek@karlin.mff.cuni.cz*
Abstract: In this thesis we deal with numerical simulations for flows of viscoelastic fluids. First, we introduce two models for viscoelastic fluids: (i) the Oldroyd-B, which is a classical model for viscoelastic fluids and (ii) a new nonlinear model which might be thought of as a generalization of Oldroyd-B to the case of large elastic deformations. Then, the flow at three different situations is discussed. The first of them is stress relaxation in parallel plate flow, which is an example of a 1D problem. The second one is a 4:1 planar contraction flow, which is a standard benchmark for viscoelastic flows. The third problem is stress relaxation in axially symmetric cylinder flow, which is solved as a 1D as well as a 2D problem. If it is possible, the problems are solved analytically, otherwise they are solved numerically with the aid of the finite element method using the software Comsol Multiphysics 3.3. Experimental data that document the stress relaxation of asphalt are available in the cylindrical geometry. Thus, finally, these data are fitted using both considered models.
Keywords: *viscoelastic fluid, asphalt, finite element method*

Chapter 1

Introduction

In the first chapter we provide basic information about the material of interest and our approach to its modeling. Then we briefly describe the experimental data on asphalt, which we use throughout this thesis. For further information about asphalt the reader is referred to [6] and [7].

1.1 About asphalt

Asphalt is a complex heterogeneous mixture of hydrocarbons. It is typically obtained as a by-product during the process of crude oil refining, but there are also natural sources of asphalt.

The most important application of asphalt is definitively the roadway and runway construction. During this process, the so-called straight run asphalt is taken from the refinery to the hot mix plant where it is mixed with aggregates and possibly other fillers and finally laid on the road. Other important uses of asphalt are e.g. insulation or storage of radioactive waste. It is also interesting to note that the natural asphalt was used even in prehistory and in the early civilizations to construct hunting equipments, in building construction and even for embalming.

In order to be able to describe the behavior of the asphalt mix used for roadway construction, it is necessary to understand the behavior of its most characteristic component which is the straight-run asphalt. This task is a difficult one because of the following reasons. Asphalt is a very complicated mixture of many different components, all of which interact with one another. The exact chemical composition and the nature of processes which take place in this mixture are still not well understood, although there is a lot of experimental evidence, that certain processes such as aging or steric and low-temperature physical hardening take place in asphalt and have a significant impact on its macroscopic behavior.

Yet another difficulty is that the behavior of asphalt depends to a large extent on the temperature. With increasing temperature asphalt can behave, roughly speaking, like a glassy solid, viscoelastic solid, viscoelastic fluid or Newtonian fluid. The precise temperature ranges for the different kinds of behavior cannot be given, because they depend to a large extent on the type and origin of asphalt. Another problem is that the behavior depends also on the timescale of observation. If a specimen is put into a funnel and left for a couple of years, a drop may fall from the stem (for more details on this exciting experiment, the reader is referred to [1]). However, when precisely the same specimen at the same temperature is hit by a hammer, it cracks in a way similar to glass.

1.2 The aim of this thesis

In this thesis we abstract from all of the above discussed complications, our aim being to capture only the most significant features of the mechanical behavior of asphalt. Therefore, we model asphalt as a single continuum (not as a mixture) at a constant temperature.

We were provided with experimental data on steady shear rate experiments with asphalt, which are described in the next section. According to the conditions of this experiment, we have decided to model asphalt as an incompressible viscoelastic fluid. We neglect the volume force, because it does not play any role in the experiment. Throughout this thesis we consider two models for such materials, namely Oldroyd-B, which is a typical model for viscoelastic fluids, and a nonlinear model, which will be introduced in the next chapter and which might be thought of as a generalization of Oldroyd-B to the case of large elastic deformations. The main objective of this thesis is to determine, in what extent these models are capable of fitting the given experimental data.

1.3 Experimental data

Now, we provide a brief description of the considered experiment, which has been conducted by Dr. J. Murali Krishnan at Indian Institute of Technology Madras [5]. Since his experimental work is still in progress, the results of his measurements have not been published yet.

The experiments were performed using a dynamic shear rheometer, their setup is shown in Figure 1.1. First, a spherical sample of asphalt was placed between the plates and was squeezed into a disc. The excess material was trimmed off. Then the specimen was allowed to relax and settle at the given

temperature. Finally, at $t = 0$ the upper plate started to rotate with a constant angular velocity ω and the corresponding torque was recorded for times $0 \leq t \leq 15\,\mathrm{s}$. The radius of the plate is $R = 4\,\mathrm{mm}$ and a constant gap of $h = 1\,\mathrm{mm}$ was maintained during the measurements. The data set contains results for temperatures of $25\,^{\circ}\mathrm{C}$ and $35\,^{\circ}\mathrm{C}$ and angular velocities of $0.125\,\mathrm{rad.s^{-1}}$, $0.25\,\mathrm{rad.s^{-1}}$ and $0.5\,\mathrm{rad.s^{-1}}$. The measured torque is plotted against time in Figure 1.2.

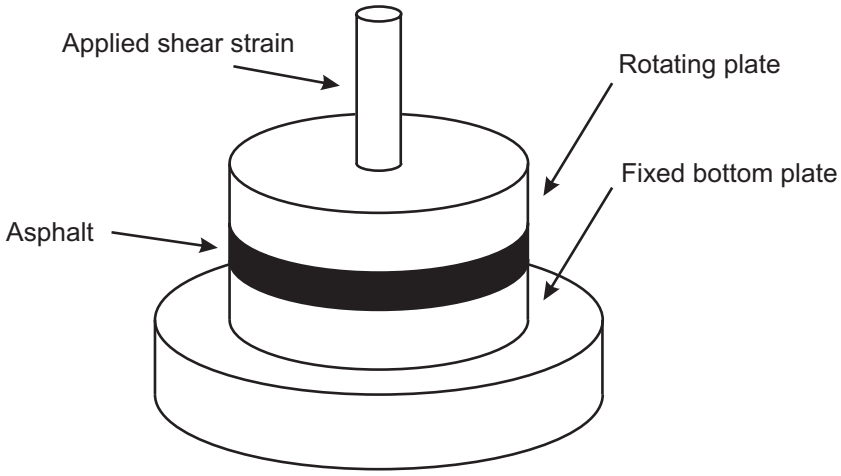

Figure 1.1: Steady shear rate experiment

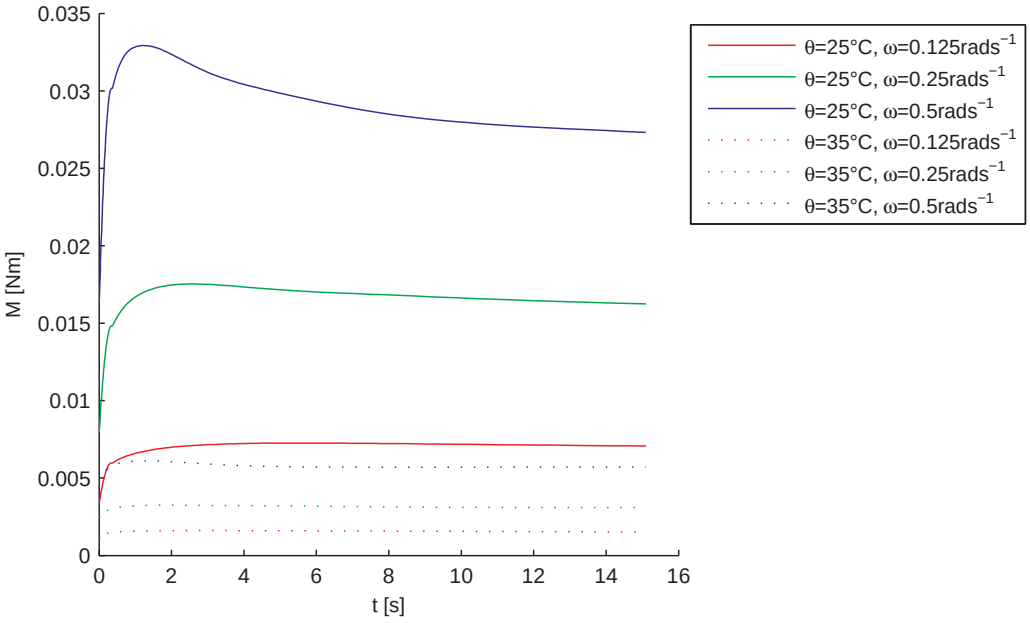

Figure 1.2: Experimental data – torque vs. time in steady shear rate experiments [5].

Chapter 2

Models for viscoelastic fluids

In this chapter we introduce two models for viscoelastic fluids, properties of which will be investigated in this thesis.

2.1 Preliminaries

For the characterization of the flow of a viscoelastic fluid we use the spatial description. Throughout the text we use the following Eulerian variables

ρ	density
$\mathbf{v}$	velocity
$\mathbf{L} = (\nabla \mathbf{v})^{\mathrm{T}}$	velocity gradient
$\mathbf{D} = \frac{1}{2}(\mathbf{L} + \mathbf{L}^{\mathrm{T}})$	rate of deformation tensor
$\mathbf{T}$	Cauchy stress tensor
$\mathbf{b}$	volume force
ϵ	specific internal energy
r	density of energy sources
$\mathbf{q}$	heat flux
η	specific entropy
θ	temperature
ψ	Helmholtz potential
ξ	rate of dissipation

The material time derivative of an Eulerian field φ is given by

$$\dot{\varphi} := \frac{\partial \varphi}{\partial t} + \mathbf{v} \cdot \nabla \varphi \,. \tag{2.1}$$

As the starting point for our discussion we summarize the balance laws of continuum mechanics in spatial description (for details see e.g. [19]):

Balance of mass

$$\dot{\rho} + \rho \operatorname{div} \mathbf{v} = 0 \tag{2.2}$$

Balance of linear momentum

$$\rho \dot{\mathbf{v}} = \rho \mathbf{b} + \operatorname{div} \mathbf{T}^{\mathrm{T}} \tag{2.3}$$

Balance of angular momentum

$$\mathbf{T} = \mathbf{T}^{\mathrm{T}} \tag{2.4}$$

Balance of internal energy

$$\rho \dot{\epsilon} = \mathbf{T} \cdot \mathbf{D} + \rho r - \operatorname{div} \mathbf{q} \tag{2.5}$$

Entropy inequality

$$\rho \dot{\eta} \geq \frac{\rho r}{\theta} - \operatorname{div} \frac{\mathbf{q}}{\theta} \tag{2.6}$$

For the later use we will express the entropy inequality in a more suitable form. Let us therefore introduce the Helmholtz free energy

$$\psi = \epsilon - \theta \eta \tag{2.7}$$

and the rate of dissipation

$$\xi = \theta \rho \dot{\eta} - \rho r + \theta \operatorname{div} \frac{\mathbf{q}}{\theta} \,. \tag{2.8}$$

It follows from (2.6) that $\xi \geq 0$ in any admissible process. On substituting ϵ from (2.7) and r from (2.5) into (2.8) we get

$$\xi = \mathbf{T} \cdot \mathbf{D} - \rho \dot{\psi} + \rho \eta \dot{\theta} - \frac{\nabla \theta}{\theta} \cdot \mathbf{q} \,. \tag{2.9}$$

Because we consider only isothermal processes, the last two terms cancel and we arrive at the final form of the energy dissipation equation

$$\xi = \mathbf{T} \cdot \mathbf{D} - \rho \dot{\psi} \,. \tag{2.10}$$

2.2 Oldroyd-B

Oldroyd-B is a standard model for viscoelastic fluids, which has been widely used for example for modeling of polymer melts and solutions. It can be

derived e.g. by considering a viscous fluid containing elastic dumbbells consisting of two spherical beads connected by a linear elastic spring. The equations of this model may be written in several different forms, we will use the following one

$$\operatorname{div} \mathbf{v} = 0 \tag{2.11a}$$

$$\rho \dot{\mathbf{v}} = \operatorname{div}(-p\mathbf{I} + 2\eta\mathbf{D} + G\mathbf{A}) \tag{2.11b}$$

$$\mathbf{A} + \tau \overset{\triangledown}{\mathbf{A}} = 2\tau\mathbf{D}\,, \tag{2.11c}$$

where $\mathbf{A}$ is the elastic extra stress tensor, $\overset{\triangledown}{\mathbf{A}} = \dot{\mathbf{A}} - \mathbf{L}\mathbf{A} - \mathbf{A}\mathbf{L}^{\mathrm{T}}$ its upper-convected Oldroyd derivative, η is viscosity, G elastic modulus and τ relaxation time. For its derivation as well as for further details on Oldroyd-B model see for example [4].

2.3 A thermodynamic framework for modeling of rate-type fluids

In this section we describe a general thermodynamic framework for modeling incompressible viscoelastic fluids. This framework proposed by Rajagopal and Srinivasa relies on the concept of natural configurations and the principle of maximal rate of dissipation. For details see e.g. [10, 9, 8].

2.3.1 Natural configurations

Besides the reference and current configurations κ_R and κ_t, we associate with the body the so-called natural configuration κ_p. In the case of an infinitesimal element of the body its meaning can be roughly explained by means of a simple linear viscoelastic model consisting of one dashpot and one spring in series. The free energy of this system is stored only in the spring. If the system is first extended by an external load and then unloaded, it goes to a 'natural' state, in which the spring is in equilibrium and thus the free energy stored in the system is equal to zero. Since the deformation of the dashpot does not change during the relaxation, we conclude that the free energy of the system depends only on the deformation from the natural state.

Now let us turn our attention to the body as a whole. Each infinitesimal element of the body has a natural state associated with it, but these natural states do not in general have to form a global configuration in the Euclidean space. For this lack of clearer physical interpretation natural configurations will be throughout this text considered merely as an abstract notion with

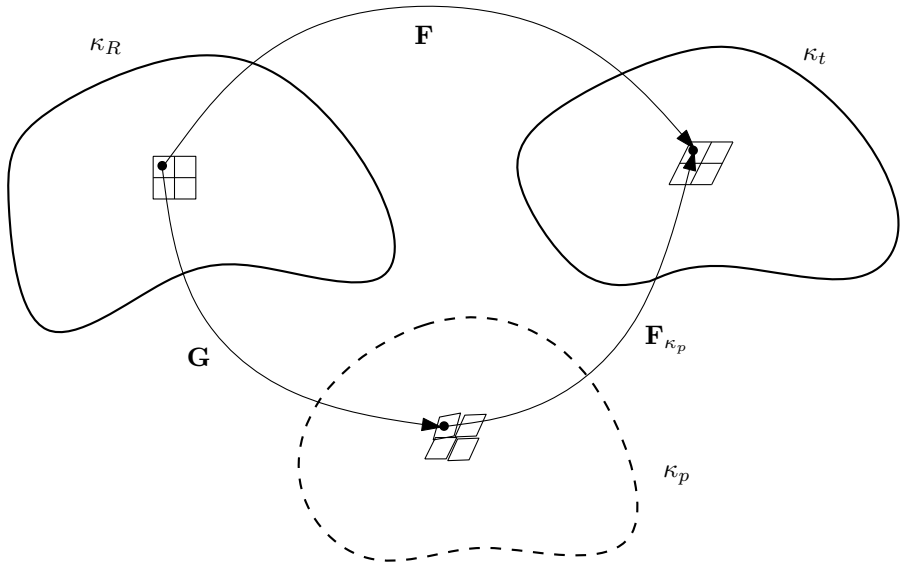

Figure 2.1: Reference, current and natural configuration and the introduction of $\mathbf{F}_{\kappa_p}$ and $\mathbf{G}$.

only conceptual meaning. For a detailed discussion of the notion of natural configurations see e.g. [11].

Now we introduce some kinematical quantities related to the natural configurations. We define $\mathbf{F}_{\kappa_p}$ as the mapping of an infinitesimal element from κ_p to κ_t and $\mathbf{G}$ as the mapping of an infinitesimal element from κ_R to κ_p. It should be pointed out that since the natural configuration is only a local notion, these two tensors are not in general gradients of any mapping and thus do not have to fulfill any compatibility conditions. They are related to $\mathbf{F}$ through

$$\mathbf{G} = \mathbf{F}_{\kappa_p}^{-1}\mathbf{F}\,. \tag{2.12}$$

Using them we define other quantities in a way, which is analogous to the definitions of quantities related to the reference configuration, namely

$$\mathbf{B}_{\kappa_p} = \mathbf{F}_{\kappa_p}\mathbf{F}_{\kappa_p}^{\mathrm{T}} \quad \text{and} \quad \mathbf{C}_{\kappa_p} = \mathbf{F}_{\kappa_p}^{\mathrm{T}}\mathbf{F}_{\kappa_p}\,, \tag{2.13}$$

as a measure of the deformation between κ_p and κ_t and

$$\mathbf{L}_{\kappa_p} = \dot{\mathbf{G}}\mathbf{G}^{-1} \quad \text{and} \quad \mathbf{D}_{\kappa_p} = \frac{\mathbf{L}_{\kappa_p} + \mathbf{L}_{\kappa_p}^{\mathrm{T}}}{2}\,. \tag{2.14}$$

as a measure of its rate.

For later use let us compute time derivatives of $\mathbf{B}_{\kappa_p}$ and its deviatoric part

$$\mathbf{B}_{\kappa_p}^{\delta} := \mathbf{B}_{\kappa_p} - \frac{1}{3}(\operatorname{tr}\mathbf{B}_{\kappa_p})\mathbf{I}\,. \tag{2.15}$$

Starting from the definition (2.13) and using the rule for product differentiation, we get first

$$\dot{\mathbf{B}}_{\kappa_p} = \left(\mathbf{F}_{\kappa_p}\mathbf{F}_{\kappa_p}^{\mathrm{T}}\right)^{\cdot} = \left(\mathbf{F}\mathbf{G}^{-1}\mathbf{G}^{-\mathrm{T}}\mathbf{F}^{\mathrm{T}}\right)^{\cdot} = \\ = \mathbf{L}\mathbf{B}_{\kappa_p} + \mathbf{B}_{\kappa_p}\mathbf{L}^{\mathrm{T}} - 2\mathbf{F}_{\kappa_p}\mathbf{D}_{\kappa_p}\mathbf{F}_{\kappa_p}^{\mathrm{T}}\,. \quad (2.16)$$

If we introduce the so–called upper convected Oldroyd derivative $\overset{\triangledown}{\mathbf{A}} = \dot{\mathbf{A}} - \mathbf{L}\mathbf{A} - \mathbf{A}\mathbf{L}^{\mathrm{T}}$, we can rewrite the last result in the final form

$$\overset{\triangledown}{\mathbf{B}}_{\kappa_p} = -2\mathbf{F}_{\kappa_p}\mathbf{D}_{\kappa_p}\mathbf{F}_{\kappa_p}^{\mathrm{T}}\,. \quad (2.17)$$

To compute the upper convected Oldroyd derivative $\overset{\triangledown}{\mathbf{B}}^{\delta}_{\kappa_p}$ we observe first that taking trace of (2.16) yields

$$\operatorname{tr}\dot{\mathbf{B}}_{\kappa_p} = 2\mathbf{D}\cdot\mathbf{B}_{\kappa_p} - 2\mathbf{C}_{\kappa_p}\cdot\mathbf{D}_{\kappa_p}\,. \quad (2.18)$$

Using that, we get straightforwardly

$$\overset{\triangledown}{\mathbf{B}}^{\delta}_{\kappa_p} = \left(\mathbf{B}_{\kappa_p} - \frac{1}{3}(\operatorname{tr}\mathbf{B}_{\kappa_p})\mathbf{I}\right)^{\triangledown} = \overset{\triangledown}{\mathbf{B}}_{\kappa_p} - \frac{1}{3}(\operatorname{tr}\dot{\mathbf{B}}_{\kappa_p})\mathbf{I} + \frac{2}{3}(\operatorname{tr}\mathbf{B}_{\kappa_p})\mathbf{D} = \\ = -2\mathbf{F}_{\kappa_p}\mathbf{D}_{\kappa_p}\mathbf{F}_{\kappa_p}^{\mathrm{T}} - \frac{2}{3}(\mathbf{D}\cdot\mathbf{B}_{\kappa_p})\mathbf{I} + \frac{2}{3}(\mathbf{C}_{\kappa_p}\cdot\mathbf{D}_{\kappa_p})\mathbf{I} + \frac{2}{3}(\operatorname{tr}\mathbf{B}_{\kappa_p})\mathbf{D}\,. \quad (2.19)$$

2.3.2 Incompressibility

The constraint of incompressibility implies that

$$\det\mathbf{F} = 1\,, \quad (2.20)$$

which upon differentiation with respect to time leads to

$$\operatorname{tr}\mathbf{D} = 0\,. \quad (2.21)$$

Since the natural configuration is also a possible state of an infinitesimal element of the body, incompressibility leads also to

$$\det\mathbf{G} = 1\,, \quad (2.22)$$

which similarly gives

$$\operatorname{tr}\mathbf{D}_{\kappa_p} = 0\,. \quad (2.23)$$

2.3.3 Principle of maximum rate of entropy production

The methodology for developing constitutive relations for incompressible rate-type fluids is the following: instead of directly prescribing a constitutive relation for the Cauchy stress tensor $\mathbf{T}$, we choose rather constitutive relations for Helmholtz free energy ψ and rate of dissipation ξ. This should be somehow 'easier', because the Cauchy stress tensor has six independent components while these quantities are only two scalars. Then, to obtain the constitutive equation for $\mathbf{T}$, we employ the principle of maximum entropy production. For the purpose of this text it can be formulated in the following way:

The values of $\mathbf{D}$ *and* $\mathbf{D}_{\kappa_p}$ *which correspond to a given value of* $\mathbf{T}$ *are those, which maximize the rate of entropy production under the constraint of reduced thermodynamic inequality and the conditions of incompressibility.*

For a detailed discussion of this principle the reader is referred for example to [12].

2.4 Model 1

Now we apply the above introduced framework to develop a model, which has been originally proposed in a more general form in [3] and which will be throughout this text referred to as Model 1.

As the first step we have to choose constitutive relations for the Helmholtz free energy and the rate of dissipation. We assume that the elastic response between κ_p and κ_t is that of a neo–Hookean material, that is

$$\hat{\psi} = \frac{\mu}{2\rho}(\operatorname{tr} \mathbf{B}_{\kappa_p} - 3)\,. \tag{2.24}$$

This is in some sense the easiest choice — ψ depends linearly on the linear invariant of $\mathbf{B}_{\kappa_p}$ and is zero if $\mathbf{B}_{\kappa_p} = \mathbf{I}$ that is if the natural configuration is equal to the current one. For the rate of dissipation we stipulate

$$\hat{\xi} = \epsilon_0 \mathbf{D} \cdot \mathbf{D} + \epsilon_1 \mathbf{D}_{\kappa_p} \cdot (\mathbf{C}_{\kappa_p} \mathbf{D}_{\kappa_p})\,, \tag{2.25}$$

the first term in this formula corresponding to the dissipation of a Newtonian fluid, the second one being responsible for viscoelastic behavior. Using (2.16) the material time derivative of ψ can be expressed as

$$\dot{\psi} = \frac{\mu}{2\rho} \operatorname{tr} \dot{\mathbf{B}}_{\kappa_p} = \frac{\mu}{\rho}(\mathbf{D} \cdot \mathbf{B}_{\kappa_p} - \mathbf{C}_{\kappa_p} \cdot \mathbf{D}_{\kappa_p})\,, \tag{2.26}$$

which upon substituting into (2.10) delivers the following form of the reduced thermodynamic inequality

$$\xi = (\mathbf{T} - \mu \mathbf{B}_{\kappa_p}) \cdot \mathbf{D} + \mu \mathbf{C}_{\kappa_p} \cdot \mathbf{D}_{\kappa_p}\,. \tag{2.27}$$

As the next step we maximize $\hat{\xi}(\mathbf{D}, \mathbf{D}_{\kappa_p})$ among the values of $\mathbf{D}$ and $\mathbf{D}_{\kappa_p}$ fulfilling the following constraints of incompressibility and the reduced thermodynamic inequality

$$0 = \operatorname{tr} \mathbf{D} \tag{2.28}$$

$$0 = \operatorname{tr} \mathbf{D}_{\kappa_p} \tag{2.29}$$

$$0 = (\mathbf{T} - \mu \mathbf{B}_{\kappa_p}) \cdot \mathbf{D} + \mu \mathbf{C}_{\kappa_p} \cdot \mathbf{D}_{\kappa_p} - \hat{\xi}(\mathbf{D}, \mathbf{D}_{\kappa_p}) \,. \tag{2.30}$$

For this purpose we adopt the method of Lagrange multipliers which delivers the following set of equations

$$\frac{\partial \hat{\xi}}{\partial \mathbf{D}} = \lambda_1 \frac{\partial}{\partial \mathbf{D}} (\xi - \hat{\xi}) + \lambda_2 \frac{\partial}{\partial \mathbf{D}} \operatorname{tr} \mathbf{D} + \lambda_3 \frac{\partial}{\partial \mathbf{D}} \operatorname{tr} \mathbf{D}_{\kappa_p} \tag{2.31}$$

$$\frac{\partial \hat{\xi}}{\partial \mathbf{D}_{\kappa_p}} = \lambda_1 \frac{\partial}{\partial \mathbf{D}_{\kappa_p}} (\xi - \hat{\xi}) + \lambda_2 \frac{\partial}{\partial \mathbf{D}_{\kappa_p}} \operatorname{tr} \mathbf{D} + \lambda_3 \frac{\partial}{\partial \mathbf{D}_{\kappa_p}} \operatorname{tr} \mathbf{D}_{\kappa_p} \tag{2.32}$$

that can be simplified to

$$\frac{1 + \lambda_1}{\lambda_1} 2\epsilon_0 \mathbf{D} = \mathbf{T} - \mu \mathbf{B}_{\kappa_p} + \frac{\lambda_2}{\lambda_1} \mathbf{I} \tag{2.33}$$

$$\frac{1 + \lambda_1}{\lambda_1} 2\epsilon_1 \mathbf{C}_{\kappa_p} \mathbf{D}_{\kappa_p} = \mu \mathbf{C}_{\kappa_p} + \frac{\lambda_3}{\lambda_1} \mathbf{I} \tag{2.34}$$

where the Lagrange multipliers λ_1, λ_2 and λ_3 have to be eliminated. To accomplish this we first make the scalar product of (2.33) with $\mathbf{D}$ and (2.34) with $\mathbf{D}_{\kappa_p}$ and sum these products. With help of (2.25) and (2.27) we easily conclude that

$$\frac{1 + \lambda_1}{\lambda_1} = \frac{1}{2} \,. \tag{2.35}$$

Next we take the trace of (2.33) and of (2.34), which delivers

$$\frac{\lambda_2}{\lambda_1} = -\frac{1}{3} \operatorname{tr}(\mathbf{T} - \mu \mathbf{B}_{\kappa_p}) \tag{2.36}$$

$$\frac{\lambda_3}{\lambda_1} = \frac{1}{3} (\epsilon_1 \mathbf{C}_{\kappa_p} \cdot \mathbf{D}_{\kappa_p} - \mu \operatorname{tr} \mathbf{C}_{\kappa_p}) \,. \tag{2.37}$$

We define the pressure as the mean normal stress

$$p = -\frac{1}{3} \operatorname{tr} \mathbf{T} \,. \tag{2.38}$$

Substitution of (2.38), (2.35), (2.36) and (2.37) into (2.33) and (2.34) yields

$$\mathbf{T} = -p\mathbf{I} + \epsilon_0 \mathbf{D} + \mu \mathbf{B}^{\delta}_{\kappa_p} \tag{2.39}$$

$$\epsilon_1 \left[\mathbf{C}_{\kappa_p} \mathbf{D}_{\kappa_p} - \frac{1}{3} (\mathbf{C}_{\kappa_p} \cdot \mathbf{D}_{\kappa_p}) \mathbf{I} \right] = \mu \left[\mathbf{C}_{\kappa_p} - \frac{1}{3} (\operatorname{tr} \mathbf{C}_{\kappa_p}) \mathbf{I} \right] \,. \tag{2.40}$$

To bring the last equation to the final form we multiply it from the left by $\mathbf{F}_{\kappa_p}^{-\mathrm{T}}$ and from the right by $\mathbf{F}_{\kappa_p}^{\mathrm{T}}$ which leads to

$$\epsilon_1 \left[\mathbf{F}_{\kappa_p} \mathbf{D}_{\kappa_p} \mathbf{F}_{\kappa_p}^{\mathrm{T}} - \frac{1}{3} (\mathbf{C}_{\kappa_p} \cdot \mathbf{D}_{\kappa_p}) \mathbf{I} \right] = \mu \left[\mathbf{F}_{\kappa_p} \mathbf{F}_{\kappa_p}^{\mathrm{T}} - \frac{1}{3} (\operatorname{tr} \mathbf{C}_{\kappa_p}) \mathbf{I} \right] \tag{2.41}$$

and using (2.19) and the fact that $\operatorname{tr} \mathbf{B}_{\kappa_p} = \operatorname{tr} \mathbf{C}_{\kappa_p}$ and $\mathbf{D} \cdot \mathbf{B}_{\kappa_p} = \mathbf{D} \cdot \mathbf{B}_{\kappa_p}^{\delta}$ to

$$\epsilon_1 \left[-\frac{1}{2} \overset{\triangledown}{\mathbf{B}}{}_{\kappa_p}^{\delta} + \frac{1}{3} (\operatorname{tr} \mathbf{B}_{\kappa_p}) \mathbf{D} - \frac{1}{3} (\mathbf{D} \cdot \mathbf{B}_{\kappa_p}^{\delta}) \mathbf{I} \right] = \mu \mathbf{B}_{\kappa_p}^{\delta} \,. \tag{2.42}$$

Finally, we introduce

$$b = \operatorname{tr} \mathbf{B}_{\kappa_p} \,, \tag{2.43}$$

which will be along with $\mathbf{B}_{\kappa_p}^{\delta}$ one of the independent variables in our model.

To summarize, we have the following set of partial differential and algebraic equations

$$\operatorname{div} \mathbf{v} = 0 \tag{2.44a}$$

$$\rho \dot{\mathbf{v}} = \operatorname{div}(-p\mathbf{I} + \epsilon_0 \mathbf{D} + \mu \mathbf{B}_{\kappa_p}^{\delta}) \tag{2.44b}$$

$$\mu \mathbf{B}_{\kappa_p}^{\delta} = \epsilon_1 \left[-\frac{1}{2} \overset{\triangledown}{\mathbf{B}}{}_{\kappa_p}^{\delta} + \frac{1}{3} b \mathbf{D} - \frac{1}{3} (\mathbf{D} \cdot \mathbf{B}_{\kappa_p}^{\delta}) \mathbf{I} \right] \tag{2.44c}$$

$$1 = \det \left(\mathbf{B}_{\kappa_p}^{\delta} + \frac{1}{3} b \mathbf{I} \right) \tag{2.44d}$$

for the independent variables p, $\mathbf{v}$, $\mathbf{B}_{\kappa_p}^{\delta}$ and b that completely characterize the state of the flow. These variables have in full 3D setting altogether ten independent components. On the other hand, equations (2.44a) and (2.44d) have both one component, equation (2.44b) three, and (2.44c), since it is symmetric and traceless, has five independent components, which makes altogether ten equations for ten unknown components.

2.5 Relationship between Model 1 and Oldroyd-B

In this section we show that under certain assumptions Model 1 reduces to Oldroyd-B. Let us therefore assume that

$$\mathbf{B}_{\kappa_p} = \mathbf{I} + \mathbf{A}, \quad \text{where} \quad |\mathbf{A}| = \varepsilon \,, \tag{2.45}$$

ε being some small parameter. Using the expansion

$$\det (\mathbf{I} + \mathbf{A}) = 1 + \operatorname{tr} \mathbf{A} + O(|\mathbf{A}|^2) \,, \tag{2.46}$$

the constraint of incompressibility $\det \mathbf{B}_{\kappa_p} = 1$ reduces under the assumption (2.45) to

$$\operatorname{tr} \mathbf{A} = 0\,, \tag{2.47}$$

which implies that

$$\operatorname{tr} \mathbf{B}_{\kappa_p} = b = 3 \quad \text{and} \quad \mathbf{B}^{\delta}_{\kappa_p} = \mathbf{A}\,. \tag{2.48}$$

In view of these results (2.44c) simplifies to

$$\mathbf{A} + \frac{\epsilon_1}{2\mu}\overset{\triangledown}{\mathbf{A}} = 2\frac{\epsilon_1}{2\mu}\mathbf{D} - \frac{\epsilon_1}{3\mu}(\mathbf{D}\cdot\mathbf{A})\mathbf{I}\,. \tag{2.49}$$

It is evident that if we further assume that also $|\mathbf{D}| = O(\varepsilon)$, the last term in this equation becomes quadratic in ϵ. Neglecting it, we arrive at

$$\mathbf{A} + \frac{\epsilon_1}{2\mu}\overset{\triangledown}{\mathbf{A}} = 2\frac{\epsilon_1}{2\mu}\mathbf{D}\,, \tag{2.50}$$

which is obviously equation (2.11c) with $\tau = \epsilon_1/2\mu$, $G = \mu$. Note that the assumption, that both $|\mathbf{B}^{\delta}_{\kappa_p}|$ and $|\mathbf{D}|$ are small actually means, that the deviatoric stress

$$\epsilon_0\mathbf{D} + \mu\mathbf{B}^{\delta}_{\kappa_p} \tag{2.51}$$

is small.

To summarize, we have shown that Model 1 and Oldroyd-B coincide for small deviatoric stresses and that the relations between the material moduli in this case are

$$\eta = \frac{\epsilon_0}{2}, \qquad \tau = \frac{\epsilon_1}{2\mu}, \qquad G = \mu\,. \tag{2.52}$$

Chapter 3

Numerical method

Now we briefly describe the method for numerical solution of partial differential equations, which will be used throughout next chapters.

3.1 Weak formulation

The starting point for the numerical solution of a problem involving partial differential equations is its weak formulation. In this section, we introduce the weak formulation of the models presented in the previous chapter in the full 3D setting.

We consider a fluid filling a given domain $\Omega \subset \mathbb{R}^3$ whose boundary $\partial\Omega$ can be separated into two parts Γ_1 and Γ_2. On Γ_1 we prescribe the Dirichlet boundary condition $\mathbf{v} = \mathbf{v}_0$ and on Γ_2 the Neumann boundary condition $\mathbf{T}\mathbf{n} = \mathbf{t}_0$, where $\mathbf{v}_0$ and $\mathbf{t}_0$ are given. Furthermore, on the inflow Γ_I (the part of the boundary where $\mathbf{v} \cdot \mathbf{n} < 0$) we have to prescribe Dirichlet condition for $\mathbf{A}$ or for $\mathbf{B}^{\delta}_{\kappa_p}$ and b.

In order to obtain the weak formulation of the equations (2.11) or (2.44) governing the flow of a viscoelastic fluid, we integrate these equations against corresponding test functions, which have zero trace on the part of the boundary where the Dirichlet condition is prescribed, and then integrate the right hand side of the momentum equation by parts taking the boundary conditions into account (see e.g. [15]).

Hence, the weak formulation of the equations for Oldroyd-B (2.11) reads

Find $(p, \mathbf{v}, \mathbf{A}) : \langle 0, T\rangle \to Q \times V \times S$ *such that*

$$\int_\Omega (\operatorname{div} \mathbf{v}) q \,\mathrm{d}\Omega = 0 \tag{3.1a}$$

$$\int_\Omega \rho \dot{\mathbf{v}} \cdot \mathbf{u} \,\mathrm{d}\Omega = \int_{\Gamma_2} \mathbf{t}_0 \cdot \mathbf{u} \,\mathrm{d}s - \int_\Omega \mathbf{T} \cdot \nabla \mathbf{u} \,\mathrm{d}\Omega \tag{3.1b}$$

$$\int_\Omega (\mathbf{A} + \tau \overset{\triangledown}{\mathbf{A}}) \cdot \mathbf{S} \,\mathrm{d}\Omega = \int_\Omega 2\tau \mathbf{D} \cdot \mathbf{S} \,\mathrm{d}\Omega \tag{3.1c}$$

for all $q \in Q$, $\mathbf{u} \in V_0$ *and* $\mathbf{S} \in S_0$.

The weak formulation of the equations for Model 1 (2.44) reads

Find $(p, \mathbf{v}, \mathbf{B}^\delta_{\kappa_p}, b) : \langle 0, T\rangle \to Q \times V \times W \times B$ *such that*

$$\int_\Omega (\operatorname{div} \mathbf{v}) q \,\mathrm{d}\Omega = 0 \tag{3.2a}$$

$$\int_\Omega \rho \dot{\mathbf{v}} \cdot \mathbf{u} \,\mathrm{d}\Omega = \int_{\Gamma_2} \mathbf{t}_0 \cdot \mathbf{u} \,\mathrm{d}s - \int_\Omega \mathbf{T} \cdot \nabla \mathbf{u} \,\mathrm{d}\Omega \tag{3.2b}$$

$$\int_\Omega \mu \mathbf{B}^\delta_{\kappa_p} \cdot \mathbf{S} \,\mathrm{d}\Omega = \int_\Omega \epsilon_1 \left[-\frac{1}{2} \overset{\triangledown}{\mathbf{B}}{}^\delta_{\kappa_p} + \frac{1}{3} b \mathbf{D} - \frac{1}{3} (\mathbf{D} \cdot \mathbf{B}^\delta_{\kappa_p}) \mathbf{I} \right] \cdot \mathbf{S} \,\mathrm{d}\Omega \tag{3.2c}$$

$$0 = \int_\Omega \left[\det \left(\mathbf{B}^\delta_{\kappa_p} + \frac{1}{3} b \mathbf{I} \right) - 1 \right] w \,\mathrm{d}\Omega \tag{3.2d}$$

for all $q \in Q$, $\mathbf{u} \in V_0$, $\mathbf{S} \in S_0$ *and* $w \in B_0$.

The above used function spaces are defined as follows.

- $Q = L^2(\Omega)$,
- V is the space of vectors with cartesian components in $W^{1,2}(\Omega)$,
- S is the space of symmetric second order tensors with cartesian components in $L^2(\Omega)$,
- W is the space of symmetric traceless second order tensors with cartesian components in $L^2(\Omega)$,
- $B = L^2(\Omega)$,

their counterparts with zero subscript denoting their subspaces with zero trace on the part of the boundary where the Dirichlet condition for the corresponding variable is prescribed.

The above presented weak formulation of Oldroyd-B is widely accepted in the area of numerical simulations (see [15, 13]) and it motivated also our derivation of the weak formulation of Model 1. However, it should be pointed out that both formulations are somewhat questionable from the mathematical

point of view, since there is neither a result concerning existence or uniqueness of solutions to these problems nor a physical principle, on which these formulations would rely. Especially problematic is the way the data on extra-stress at the inflow boundary, which are needed to completely characterize the state of the fluid inside the domain, are taken into account. In order to be able to speak about the value of the extra-stress on the boundary, we need to know that it lies in a space where the trace of a function is well defined. This is not the case in $L^2(\Omega)$, however, the theory of hyperbolic equations in one spatial dimension indicates that the extra-stress might lie in some better space such as $L^2(\Omega) \cap BV(\Omega)$, where the trace may be defined in some generalized sense. In any case, a reasonable mathematical theory for the equations (2.11) or (2.44) still needs to be developed. For an overview of known results concerning this analysis, we refer the reader for example to [15].

3.2 Solution method and software

We solve our equations with the Finite Element Method, i.e we start with the weak formulation of a given problem, discretise it in terms of the Galerkin method and then solve the corresponding system of algebraic equations.

For this purpose we employ Comsol Multiphysics 3.3. For a detailed description of the numerical schemes used by this software we refer to [2]. Its most important features according to this reference are listed below.

Linear solver To solve linear algebraic systems, Comsol uses the direct solver UMFPACK [17, 16].

Nonlinear solver To solve nonlinear algebraic systems, Comsol uses a solver based on an affine invariant form of the damped Newton method.

Time dependent solver To solve time dependent problems, Comsol uses a version of the DAE solver DASPK, which uses variable-order variable-stepsize backward differentiation formulas. Thus the solver is an implicit time-stepping scheme, which implies that it must solve a possibly nonlinear system of equations at each time step. It solves the nonlinear system using a Newton iteration.

For problems with one spatial dimension we discretise the domain (interval) using equidistant segments, for problems with two spatial dimensions we use a quadrilateral mesh consisting of rectangles. The shape functions are piecewise linear discontinuous for pressure and continuous piecewise quadratic for all other variables. This choice satisfies the Babuška-Brezzi condition and leads at least in the case of Oldroyd-B to a stable numerical scheme (see [15]).

Chapter 4

Parallel plate flow

In this chapter we investigate the response of the above-presented models in the most trivial case which is the flow between two parallel plates. This geometry is a one-dimensional analogy of the experiment described in Section 1.3 and therefore it helps us to understand some of the problems which we encounter later in the cylindrical geometry.

4.1 Problem description

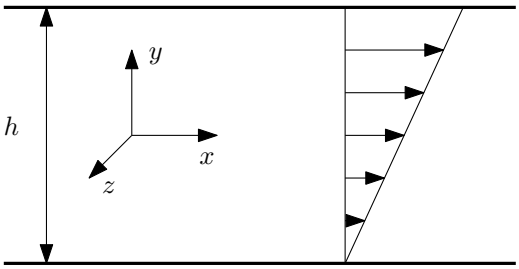

Figure 4.1: Flow between parallel plates

The geometry of the flow is shown in Figure 4.1, for its description we employ cartesian coordinates with the x-axis coinciding with the flow direction. In order to reduce the system of partial differential equations governing the flow to a set of ordinary differential equations, it is assumed that the components of velocity and elastic stress depend only on the y coordinate. Furthermore, the velocity is assumed to be parallel with the plates.

In the steady case, we deal with the so-called Couette flow driven by the motion of the upper plate and the Poiseuille flow driven by an externally imposed pressure gradient (see [14]). Furthermore, we investigate the capability of both models to capture the non-Newtonian effects of shear thinning/thickening and normal stress difference by examining the generalized

viscosity

$$\eta_g = \frac{T_{xy}}{\frac{\partial v_x}{\partial y}} \tag{4.1}$$

and the first and second normal stress differences

$$N_1 = T_{xx} - T_{yy}, \quad N_2 = T_{yy} - T_{zz}\,. \tag{4.2}$$

In the unsteady case, we restrict our attention to stress relaxation, i.e. we prescribe the boundary conditions

$$v_x(t,0) = 0, \quad v_x(t,h) = v_0 H(t)\,, \tag{4.3}$$

and the initial conditions

$$\mathbf{v}(0,\mathbf{x}) = 0 \tag{4.4a}$$
$$\mathbf{A}(0,\mathbf{x}) = 0 \text{ for Oldroyd-B} \tag{4.4b}$$
$$\mathbf{B}^{\delta}_{\kappa_p}(0,\mathbf{x}) = 0 \text{ and } b(0,\mathbf{x}) = 3 \text{ for Model 1} \tag{4.4c}$$

and we are interested in the corresponding shear stress. Here $H(t)$ denotes the Heaviside (unit step) function.

4.2 Oldroyd-B

4.2.1 Steady flow

Substituting the ansatz [1]

$$p = p(x), \quad \mathbf{v} = \begin{pmatrix} v_x(y) \\ 0 \\ 0 \end{pmatrix}, \quad \mathbf{A} = \begin{pmatrix} A_{xx}(y) & A_{xy}(y) & 0 \\ A_{xy}(y) & 0 & 0 \\ 0 & 0 & 0 \end{pmatrix} \tag{4.5}$$

into the equations for Oldroyd-B (2.11), we obtain

$$0 = -\frac{\partial p}{\partial x} + \eta \frac{\partial^2 v_x}{\partial y^2} + G \frac{\partial A_{xy}}{\partial y} \tag{4.6a}$$
$$A_{xx} - 2\tau A_{xy} \frac{\partial v_x}{\partial y} = 0 \tag{4.6b}$$
$$A_{xy} = \tau \frac{\partial v_x}{\partial y}\,, \tag{4.6c}$$

[1] Note that the fact that some of the components of the tensor $\mathbf{A}$ are equal to zero follows directly form the governing equations. We assume that they are zero apriori just in order to make the computation more transparent.

the remaining equations being identically fulfilled. Now substitution of (4.6c) into (4.6b) and (4.6a) gives

$$A_{xx} = 2\tau^2 \left(\frac{\partial v_x}{\partial y}\right)^2 \tag{4.7}$$

$$\frac{\partial p}{\partial x} = (\eta + G\tau)\frac{\partial^2 v_x}{\partial y^2}. \tag{4.8}$$

Since the left-hand side of the last equation depends only on x while the right-hand side only on y, they both must be equal to the same constant, say $-k$. Thus, the pressure varies linearly along the channel

$$p = p_0 - kx, \quad p_0 = \text{const}\,. \tag{4.9}$$

We discuss two special cases in what follows.

Plane Poiseuille flow

Poiseuille flow is driven by the pressure gradient, i.e,

$$-\frac{\partial p}{\partial x} = k \neq 0, \quad v_x(0) = v_x(h) = 0\,. \tag{4.10}$$

Consequently, it follows from (4.8) that

$$(\eta + G\tau)\frac{\partial^2 v_x}{\partial y^2} = -k\,. \tag{4.11}$$

Integrating this equation twice and taking the boundary conditions (4.10) into account, we obtain

$$v_x = \frac{k}{2(\eta + G\tau)} y(h - y)\,, \tag{4.12}$$

and then (4.6b) and (4.6c) lead to

$$A_{xx} = \frac{\tau^2 k^2}{2(\eta + G\tau)^2}(h - 2y)^2 \tag{4.13}$$

$$A_{xy} = \frac{\tau k}{2(\eta + G\tau)}(h - 2y)\,. \tag{4.14}$$

Plane Couette flow

Couette flow is driven by the motion of the upper plate at a constant pressure, i.e

$$\frac{\partial p}{\partial x} = k = 0, \quad v_x(0) = 0, \quad v_x(h) = v_0\,. \tag{4.15}$$

From (4.6) and (4.8) we easily conclude that

$$v_x = \frac{v_0 y}{h} \tag{4.16}$$

$$A_{xx} = 2\left(\frac{v_0\tau}{h}\right)^2 \tag{4.17}$$

$$A_{xy} = \frac{v_0\tau}{h}\,. \tag{4.18}$$

The shear stress at the upper plate is

$$T_{xy} = (\eta + G\tau)\frac{v_0}{h}\,. \tag{4.19}$$

Finally, let us investigate the viscometric functions of the flow. The generalized viscosity is

$$\eta_g = \frac{T_{xy}}{\frac{\partial v_x}{\partial y}} = \eta + G\tau \tag{4.20}$$

and is constant, the first normal stress difference

$$N_1 = T_{xx} - T_{yy} = 2\tau^2\left(\frac{\partial v_x}{\partial y}\right)^2 \tag{4.21}$$

is nonzero whereas the second normal stress difference

$$N_2 = T_{yy} - T_{zz} \tag{4.22}$$

is zero.

4.2.2 Unsteady flow

Assuming that

$$p = p(t), \quad \mathbf{v} = \begin{pmatrix} v_x(t,y) \\ 0 \\ 0 \end{pmatrix}, \quad \mathbf{A} = \begin{pmatrix} A_{xx}(t,y) & A_{xy}(t,y) & 0 \\ A_{xy}(t,y) & 0 & 0 \\ 0 & 0 & 0 \end{pmatrix}, \tag{4.23}$$

the Oldroyd-B model (2.11) leads to

$$\rho\frac{\partial v_x}{\partial t} = \eta\frac{\partial^2 v_x}{\partial y^2} + G\frac{\partial A_{xy}}{\partial y} \tag{4.24a}$$

$$A_{xx} + \tau\left(\frac{\partial A_{xx}}{\partial t} - 2A_{xy}\frac{\partial v_x}{\partial y}\right) = 0 \tag{4.24b}$$

$$A_{xy} + \tau\frac{\partial A_{xy}}{\partial t} = \tau\frac{\partial v_x}{\partial y}\,. \tag{4.24c}$$

These equations together with the boundary and initial conditions (4.3) and (4.4) do not have any simple analytical solution, therefore we derive their weak formulation

$$\int_0^h \rho\frac{\partial v_x}{\partial t}u_x\,\mathrm{d}y = -\int_0^h \eta\frac{\partial v_x}{\partial y}\frac{\partial u_x}{\partial y} + GA_{xy}\frac{\partial u_x}{\partial y}\,\mathrm{d}y \tag{4.25a}$$

$$\int_0^h \tau\frac{\partial A_{xx}}{\partial t}S_{xx}\,\mathrm{d}y = \int_0^h \left(2\tau A_{xy}\frac{\partial v_x}{\partial y} - A_{xx}\right)S_{xx}\,\mathrm{d}y \tag{4.25b}$$

$$\int_0^h \tau\frac{\partial A_{xy}}{\partial t}S_{xy}\,\mathrm{d}y = \int_0^h \left(\tau\frac{\partial v_x}{\partial y} - A_{xy}\right)S_{xy}\,\mathrm{d}y \tag{4.25c}$$

and solve them numerically. For the discussion of the numerical results see Section 4.4.

However, if we approximate the velocity by

$$v_x(t,y) = \frac{v_0(t)y}{h} \tag{4.26}$$

and neglect the time derivative of $v_0(t)$, the equations (4.24) simplify to

$$0 = G\frac{\partial A_{xy}}{\partial y} \tag{4.27a}$$

$$A_{xx} + \tau\left(\frac{\partial A_{xx}}{\partial t} - \frac{2v_0}{h}A_{xy}\right) = 0 \tag{4.27b}$$

$$A_{xy} + \tau\frac{\partial A_{xy}}{\partial t} = \frac{\tau v_0}{h} \tag{4.27c}$$

and have the following analytical solution

$$A_{xx} = 2\left(\frac{v_0\tau}{h}\right)^2\left[1 - \left(1 + \frac{t}{\tau}\right)e^{-t/\tau}\right] \tag{4.28}$$

$$A_{xy} = \frac{v_0\tau}{h}\left(1 - e^{-t/\tau}\right). \tag{4.29}$$

The shear stress at the upper plate is given by

$$T_{xy} = \frac{v_0}{h}\left[\eta + G\tau(1 - e^{-t/\tau})\right]\,. \tag{4.30}$$

4.3 Model 1

Now we investigate the behavior of Model 1 in an analogous way.

4.3.1 Steady flow

Substituting the choice

$$p = p(x,y), \quad \mathbf{v} = \begin{pmatrix} v_x(y) \\ 0 \\ 0 \end{pmatrix}, \quad b = b(y) \tag{4.31a}$$

$$\mathbf{B}^{\delta}_{\kappa_p} = \begin{pmatrix} B^{\delta}_{xx}(y) & B^{\delta}_{xy}(y) & 0 \\ B^{\delta}_{xy}(y) & B^{\delta}_{yy}(y) & 0 \\ 0 & 0 & -B^{\delta}_{xx}(y) - B^{\delta}_{yy}(y) \end{pmatrix} \tag{4.31b}$$

into the equations for Model 1 (2.44), we obtain

$$0 = -\frac{\partial p}{\partial x} + \frac{\epsilon_0}{2}\frac{\partial^2 v_x}{\partial y^2} + \mu\frac{\partial B^{\delta}_{xy}}{\partial y} \tag{4.32a}$$

$$0 = -\frac{\partial p}{\partial y} + \mu\frac{\partial B^{\delta}_{yy}}{\partial y} \tag{4.32b}$$

$$\mu B^{\delta}_{xx} = \frac{2\epsilon_1}{3}\frac{\partial v_x}{\partial y}B^{\delta}_{xy} \tag{4.32c}$$

$$\mu B^{\delta}_{xy} = \frac{\epsilon_1}{2}\frac{\partial v_x}{\partial y}B^{\delta}_{yy} + \frac{\epsilon_1}{6}\frac{\partial v_x}{\partial y}b \tag{4.32d}$$

$$\mu B^{\delta}_{yy} = -\frac{\epsilon_1}{3}\frac{\partial v_x}{\partial y}B^{\delta}_{xy} \tag{4.32e}$$

$$1 = \left[\left(B^{\delta}_{xx} + \frac{b}{3}\right)\left(B^{\delta}_{yy} + \frac{b}{3}\right) - {B^{\delta}_{xy}}^2\right]\left(-B^{\delta}_{xx} - B^{\delta}_{yy} + \frac{b}{3}\right) \tag{4.32f}$$

First let us deal with equations concerning $\mathbf{B}_{\kappa_p}$ that is with (4.32c)–(4.32f). From equations (4.32c) to (4.32e), it follows that

$$B^{\delta}_{xx} = \frac{4\alpha}{3}B^{\delta}_{xy} \tag{4.33}$$

$$B^{\delta}_{yy} = -\frac{2\alpha}{3}B^{\delta}_{xy} \tag{4.34}$$

$$b = \left(2\alpha + \frac{3}{\alpha}\right)B^{\delta}_{xy}\,, \tag{4.35}$$

where for the simplicity of notation we have defined

$$\alpha := \frac{\epsilon_1}{2\mu}\frac{\partial v_x}{\partial y}\,. \tag{4.36}$$

Substituting these results into the equation (4.32f) leads to a cubic equation for B^{δ}_{xy}, the only real solution of which is

$$B^{\delta}_{xy} = \frac{\alpha}{\sqrt[3]{1+\alpha^2}}\,. \tag{4.37}$$

Now let us turn our attention to the momentum equations (4.32a)–(4.32b). Integration of (4.32b) with respect to y yields

$$p = \mu B^{\delta}_{yy} + p^*(x)\,, \tag{4.38}$$

where $p^*(x)$ is an arbitrary function of x. Substitution of this result into (4.32a) gives

$$\frac{\partial p^*}{\partial x} = \frac{\partial}{\partial y}\left(\frac{\epsilon_0}{2}\frac{\partial v_x}{\partial y} + \mu B^{\delta}_{xy}\right)\,. \tag{4.39}$$

Since the left-hand side of this equation depends only on x while the right-hand side depends only on y, they both must be equal to the same constant, say $-k$. This implies firstly

$$p^* = kx + p_0, \quad p_0 = \text{const}\,. \tag{4.40}$$

and secondly

$$\frac{\partial}{\partial y}\left(\frac{\epsilon_0}{2}\frac{\partial v_x}{\partial y} + \mu B^{\delta}_{xy}\right) = k\,. \tag{4.41}$$

As in the case of Oldroyd-B, we shall resolve two special cases.

Plane Poiseuille flow

Upon substituting B^{δ}_{xy} into (4.41) we obtain

$$\frac{\partial}{\partial y}\left[\frac{\partial v_x}{\partial y}\left(\frac{\epsilon_0}{2} + \frac{\epsilon_1}{2}\frac{1}{\sqrt[3]{1+\left(\frac{\epsilon_1}{2\mu}\frac{\partial v_x}{\partial y}\right)^2}}\right)\right] = k\,, \tag{4.42}$$

which together with the boundary conditions (4.10) forms a boundary value problem for the velocity profile $v_x(y)$. Since it does not allow an analytical solution, we derive its weak form

$$\int_0^h \frac{\partial v_x}{\partial y}\left(\frac{\epsilon_0}{2} + \frac{\epsilon_1}{2}\frac{1}{\sqrt[3]{1+\left(\frac{\epsilon_1}{2\mu}\frac{\partial v_x}{\partial y}\right)^2}}\right)\frac{\partial u_x}{\partial y}\,\mathrm{d}y = \int_0^h ku\,\mathrm{d}y \tag{4.43}$$

and solve it numerically. We will discuss the results in Section 4.4.

Plane Couette flow

Again, substituting B^{δ}_{xy} into (4.41), setting $k = 0$ and integrating with respect to y, we obtain

$$\frac{\partial v_x}{\partial y}\left(\frac{\epsilon_0}{2} + \frac{\epsilon_1}{2}\frac{1}{\sqrt[3]{1+\left(\frac{\epsilon_1}{2\mu}\frac{\partial v_x}{\partial y}\right)^2}}\right) = C_1\,, \tag{4.44}$$

which can be considered as an algebraic equation for $\frac{\partial v_x}{\partial y}$. Since C_1 is a constant, $\frac{\partial v_x}{\partial y}$ must be also constant, which implies that the velocity profile is linear and in view of the chosen boundary conditions (4.15) has the form

$$v_x = \frac{v_0}{h}y\,. \tag{4.45}$$

Let us now investigate the viscometric functions of the flow. The generalized viscosity is

$$\eta_g = \frac{T_{xy}}{\frac{\partial v_x}{\partial y}} = \frac{\epsilon_0}{2} + \frac{\epsilon_1}{2}\frac{1}{\sqrt[3]{1+\alpha^2}} \tag{4.46}$$

and is a monotonically decreasing function of shear rate which means that Model 1 exhibits shear thinning. Like in the case of Oldroyd-B model, the first normal stress difference

$$N_1 = T_{xx} - T_{yy} = \frac{2\alpha^2}{\sqrt[3]{1+\alpha^2}} \tag{4.47}$$

is nonzero whereas the second normal stress difference

$$N_2 = T_{yy} - T_{zz} \tag{4.48}$$

is zero.

4.3.2 Unsteady flow

Substituting the choices

$$p = p(t,x,y), \quad \mathbf{v} = \begin{pmatrix} v_x(t,y) \\ 0 \\ 0 \end{pmatrix}, \quad b = b(t,y) \tag{4.49a}$$

$$\mathbf{B}^{\delta}_{\kappa_p} = \begin{pmatrix} B^{\delta}_{xx}(t,y) & B^{\delta}_{xy}(t,y) & 0 \\ B^{\delta}_{xy}(t,y) & B^{\delta}_{yy}(t,y) & 0 \\ 0 & 0 & -B^{\delta}_{xx}(t,y) - B^{\delta}_{yy}(t,y) \end{pmatrix} \tag{4.49b}$$

into the equations for Model 1 (2.44), we obtain

$$\rho\frac{\partial v_x}{\partial t} = -\frac{\partial p}{\partial x} + \frac{\epsilon_0}{2}\frac{\partial^2 v_x}{\partial y^2} + \mu\frac{\partial B^\delta_{xy}}{\partial y} \tag{4.50a}$$

$$0 = -\frac{\partial p}{\partial y} + \mu\frac{\partial B^\delta_{yy}}{\partial y} \tag{4.50b}$$

$$\mu B^\delta_{xx} = \epsilon_1\left(-\frac{1}{2}\frac{\partial B^\delta_{xx}}{\partial t} + \frac{2}{3}\frac{\partial v_x}{\partial y}B^\delta_{xy}\right) \tag{4.50c}$$

$$\mu B^\delta_{xy} = \epsilon_1\left(-\frac{1}{2}\frac{\partial B^\delta_{xy}}{\partial t} + \frac{1}{2}\frac{\partial v_x}{\partial y}B^\delta_{yy} + \frac{1}{6}\frac{\partial v_x}{\partial y}b\right) \tag{4.50d}$$

$$\mu B^\delta_{yy} = \epsilon_1\left(-\frac{1}{2}\frac{\partial B^\delta_{yy}}{\partial t} - \frac{1}{3}\frac{\partial v_x}{\partial y}B^\delta_{xy}\right) \tag{4.50e}$$

$$1 = \left[\left(B^\delta_{xx} + \frac{b}{3}\right)\left(B^\delta_{yy} + \frac{b}{3}\right) - {B^\delta_{xy}}^2\right]\left(-B^\delta_{xx} - B^\delta_{yy} + \frac{b}{3}\right). \tag{4.50f}$$

Adding up (4.50c) and the double of (4.50e) yields

$$\mu(B^\delta_{xx} + 2B^\delta_{yy}) = -\frac{\epsilon_1}{2}\frac{\partial}{\partial t}(B^\delta_{xx} + 2B^\delta_{yy}) \tag{4.51}$$

which in view of the initial conditions for $\mathbf{B}_{\kappa_p}$ (4.4c) implies that

$$B^\delta_{xx} = -2B^\delta_{yy}\,. \tag{4.52}$$

Similarly as in the steady case we conclude from the momentum equations (4.50a)–(4.50b) that

$$p = \mu B^\delta_{yy} - kx + p_0\,, \tag{4.53}$$

where $k = \text{const}\,.$ is an externally imposed pressure gradient which will be in this subsection considered zero. In view of these results (4.50) simplifies to

$$\rho\frac{\partial v_x}{\partial t} = \frac{\epsilon_0}{2}\frac{\partial^2 v_x}{\partial y^2} + \mu\frac{\partial B^\delta_{xy}}{\partial y} \tag{4.54a}$$

$$\mu B^\delta_{xy} = \epsilon_1\left(-\frac{1}{2}\frac{\partial B^\delta_{xy}}{\partial t} + \frac{1}{2}\frac{\partial v_x}{\partial y}B^\delta_{yy} + \frac{1}{6}\frac{\partial v_x}{\partial y}b\right) \tag{4.54b}$$

$$\mu B^\delta_{yy} = \epsilon_1\left(-\frac{1}{2}\frac{\partial B^\delta_{yy}}{\partial t} - \frac{1}{3}\frac{\partial v_x}{\partial y}B^\delta_{xy}\right) \tag{4.54c}$$

$$1 = \left[\left(-2B^\delta_{yy} + \frac{b}{3}\right)\left(B^\delta_{yy} + \frac{b}{3}\right) - {B^\delta_{xy}}^2\right]\left(B^\delta_{yy} + \frac{b}{3}\right). \tag{4.54d}$$

Unfortunately, we did not find any exact or approximate solution to this system and thus we have to solve it numerically. Its weak form is

$$\int_0^h \rho \frac{\partial v_x}{\partial t} u_x \,\mathrm{d}y = -\int_0^h \left(\frac{\epsilon_0}{2} \frac{\partial v_x}{\partial y} + \mu B_{xy}^{\delta} \right) \frac{\partial u_x}{\partial y} \,\mathrm{d}y \tag{4.55a}$$

$$\int_0^h \frac{\epsilon_1}{2} \frac{\partial B_{xy}^{\delta}}{\partial t} W_{xy} \,\mathrm{d}y = \int_0^h \left(-\mu B_{xy}^{\delta} + \frac{\epsilon_1}{2} \frac{\partial v_x}{\partial y} B_{yy}^{\delta} + \frac{\epsilon_1}{6} \frac{\partial v_x}{\partial y} b \right) W_{xy} \,\mathrm{d}y \tag{4.55b}$$

$$\int_0^h \frac{\epsilon_1}{2} \frac{\partial B_{yy}^{\delta}}{\partial t} W_{yy} \,\mathrm{d}y = \int_0^h \left(-\mu B_{yy}^{\delta} - \frac{\epsilon_1}{2} \frac{\partial v_x}{\partial y} B_{xy}^{\delta} \right) W_{yy} \,\mathrm{d}y \tag{4.55c}$$

$$0 = \int_0^h \left\{ \left[\left(-2B_{yy}^{\delta} + \frac{b}{3} \right) \left(B_{yy}^{\delta} + \frac{b}{3} \right) - {B_{xy}^{\delta}}^2 \right] \left(B_{yy}^{\delta} + \frac{b}{3} \right) - 1 \right\} w \,\mathrm{d}y \tag{4.55d}$$

and the numerical results along with the results for Oldroyd-B are discussed in the next section.

4.4 Numerical results

Firstly, we have computed the velocity profiles for the Poiseuille flow in dependence on the relaxation time, see Figure 4.2 for details. The results for Model 1 were obtained by solving equation (4.43) with the aid of finite elements, the results for Oldroyd-B using the formula (4.12). We see that for low values of relaxation time the velocity profiles for both models are identical. As the relaxation time increases, the velocity in Model 1 becomes higher than in Oldroyd-B, its profile being still almost quadratic. A profile which differs significantly from a parabola was obtained only for unrealisticly high relaxation times or pressure gradients.

Then, we have carried out time dependent numerical simulations of the stress relaxation in Oldroyd-B and Model 1 using the equations (4.25) and (4.55) respectively. The distance of the plates was taken $h = 10^{-3}\,\mathrm{mm}$ and considered values of the material moduli were of the same order of magnitude as in the experiment described in Section 1.3. The Heaviside function in the boundary condition was smoothened over a finite interval $10^{-15}\,\mathrm{s}$. Spatial discretisation was $h_0 = h/100$, the time step varied between $10^{-15}\,\mathrm{s}$ after the start and $10^{-3}\,\mathrm{s}$ at the end of the time interval.

We were first interested in the development of the velocity profile. It turned out that a linear velocity profile establishes in both models very quickly, for the values corresponding to the experiment approximately in $10^{-8}\,\mathrm{s}$. Therefore, there is no difference between the numerical solution of the flow for Oldroyd-B and the corresponding approximate solution (4.30), except for the time before the linear profile establishes. Within this interval

the computed shear stress is noticeably larger, because the velocity gradient at the top plate is larger than in the linear profile. When we smoothened the Heaviside function over a longer time interval, say 10^{-5} s, the velocity profile was linear throughout the whole simulation.

Then, we focused our interest on the kind of response the models can actually exhibit. Figures 4.3 and 4.4 show the response of both models for different values of the upper plate velocity and relaxation time respectively. In both cases we have observed that for lower values of shear stress to which also lower norms of $\mathbf{A}$ and $\mathbf{B}_{\kappa_p}$ correspond, the response of both models is equal. With increasing torque we observe firstly that the shear stress for Model 1 is lower than for Oldroyd-B, and secondly that Model 1 starts to exhibit overshoots in torque, which Oldroyd-B never does.

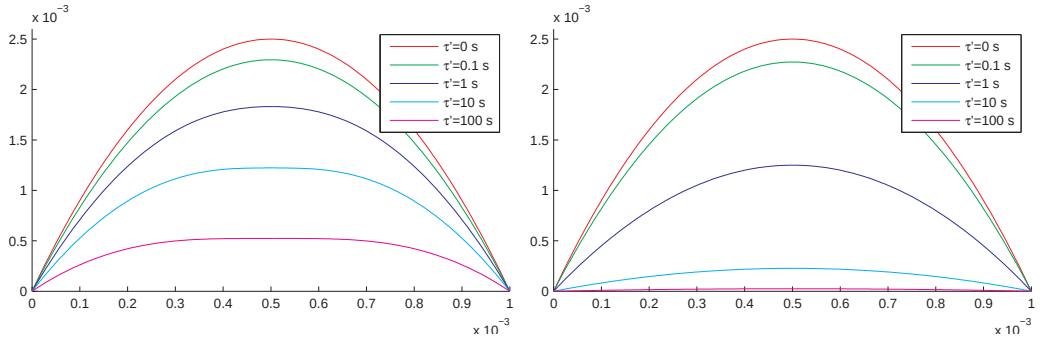

Figure 4.2: Velocity profiles in plane Poiseuille flow for Oldroyd-B (left) and Model 1 (right) for varying value of the relaxation time ($k = 10^9$ Pa, $\eta = 5.10^4$ Pa.s, $G = 10^5$ Pa, $\tau = \tau'$ resp. $\epsilon_0 = 10^5$ Pa.s, $\epsilon_1 = 2\mu\tau'$, $\mu = 10^5$ Pa)

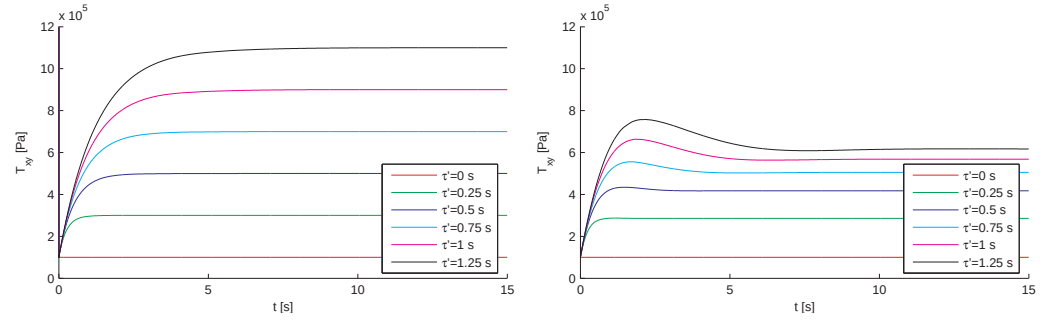

Figure 4.3: Shear stress for Oldroyd-B (left) and Model 1 (right) for varying value of the relaxation time ($v_0 = 2\,\text{mm.s}^{-1}$, $\eta = 5.10^4$ Pa.s, $G = 10^5$ Pa, $\tau = \tau'$ resp. $\epsilon_0 = 10^5$ Pa.s, $\epsilon_1 = 2\mu\tau'$, $\mu = 10^5$ Pa)

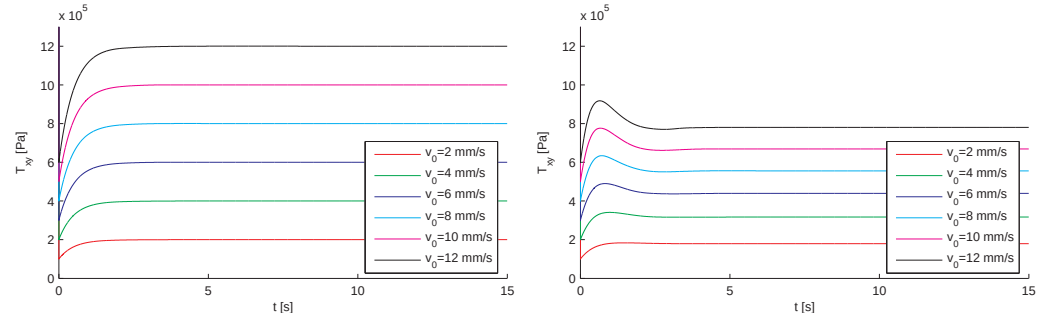

Figure 4.4: Shear stress for Oldroyd-B (left) and Model 1 (right) for varying upper plate velocity ($\eta = 5.10^4$ Pa.s, $G = 10^5$ Pa, $\tau = 0.2$ s resp. $\epsilon_0 = 10^5$ Pa.s, $\epsilon_1 = 10^5$ Pa.s, $\mu = 10^5$ Pa)

Chapter 5

Planar contraction flow

As the second example we have chosen the planar 4:1 contraction flow of an Oldroyd-B fluid, which is a standard benchmark problem in viscoelasticity. Our aim in this example is to obtain some results, which allow comparison with the literature. For this purpose we have chosen the paper [18], where a solution to this benchmark problem is presented and compared with results established earlier by several other authors.

5.1 Problem description

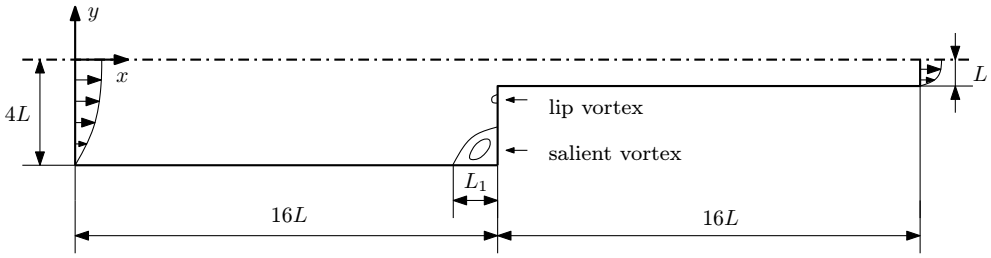

Figure 5.1: The contraction flow geometry.

The geometry for the 4:1 contraction is shown in figure 5.1. The symmetry is assumed along $y = 0$ which allows us to seek a solution only for $y \leq 0$. The fluid passes from a channel of half width $4L$ to a channel of half width L. The length of both upstream and downstream channel is $16L$. We look for steady state solution.

For the sake of easier comparison of our results with [18] we rewrite the equations for Oldroyd-B model (2.11) into the form used in this paper. There-

fore, we introduce the following non-dimensional quantities

$$v_i^* = \frac{v_i}{L}\,, \quad x_i^* = \frac{x_i}{L}\,, \quad t^* = \frac{Ut}{L} \tag{5.1}$$

$$p^* = \frac{L}{U(\eta + G\tau)}p\,, \quad \boldsymbol{\tau}_1^* = \frac{GL}{U(\eta + G\tau)}\mathbf{A}\,, \tag{5.2}$$

where U is the average velocity in the downstream channel, and substitute them into (2.11), which after dropping the stars by the non-dimensional quantities gives

$$\operatorname{div}\mathbf{v} = 0 \tag{5.3a}$$

$$\operatorname{Re}\dot{\mathbf{v}} = -\nabla p + \operatorname{div}\boldsymbol{\tau}_1 + \beta\Delta\mathbf{v} \tag{5.3b}$$

$$\boldsymbol{\tau}_1 + \operatorname{We}\overset{\triangledown}{\boldsymbol{\tau}}_1 = (1-\beta)(\nabla\mathbf{v} + \nabla\mathbf{v}^{\mathrm{T}})\,. \tag{5.3c}$$

The Reynolds and Weissenberg numbers and the parameter β are defined by

$$\operatorname{Re} = \frac{\rho UL}{\eta + G\tau}, \qquad \operatorname{We} = \frac{\tau U}{L}, \qquad \beta = \frac{\eta}{\eta + G\tau}\,, \tag{5.4}$$

according to [18] we consider $\beta = 1/9$ throughout this chapter. For further comparison, we define also the extra stress $\boldsymbol{\tau}$ by

$$\boldsymbol{\tau} = \boldsymbol{\tau}_1 + 2\beta\mathbf{D}. \tag{5.5}$$

The prescribed boundary conditions are the following: fully developed flow is imposed on the inlet through

$$v_x = \frac{3}{128}(16 - y^2), \qquad v_y = 0 \tag{5.6}$$

$$\tau_{1xx} = \frac{9}{2048}\operatorname{We}(1-\beta)y^2, \qquad \tau_{1yy} = 0, \qquad \tau_{1xy} = -\frac{3}{64}(1-\beta)y \tag{5.7}$$

and on the outlet by

$$T_{xy} = 0, \qquad v_y = 0\,. \tag{5.8}$$

No–slip conditions

$$v_x = 0, \qquad v_y = 0 \tag{5.9}$$

are imposed on solid boundaries and symmetry conditions

$$\frac{\partial v_x}{\partial y} = 0, \qquad v_y = 0 \tag{5.10}$$

on the axis of symmetry.

5.2 Numerical method

5.2.1 Artificial diffusion

During the solution we have found out that there are spurious oscillations in $\boldsymbol{\tau}_1$ which are caused by the singularity in the re-entrant corner. These oscillations caused the numerical solution to breakdown for Weissenberg numbers greater than approximately 0.5. In order to solve the equations for higher values of We , the equations (5.3) needed to be stabilized. We have performed numerical experiments with three different stabilization schemes, namely isotropic diffusion, streamline upwinding Petrov-Galerkin method and streamline diffusion, the last one giving the best results. Therefore, we discuss only the results obtained with this method.

To stabilize the equations (5.3) using the streamline diffusion, we add an additional term to the momentum and elastic stress transport equations, which represents diffusion in the direction of streamlines

$$\mathrm{Re}\,\dot{\mathbf{v}} = -\nabla p + \beta\Delta\mathbf{v} + \mathrm{div}\,\boldsymbol{\tau}_1 + \mathrm{div}\left(\frac{\delta h_0}{|\mathbf{v}|^2}(\mathbf{v}\otimes\mathbf{v})\nabla\mathbf{v}\right) \tag{5.11a}$$

$$\boldsymbol{\tau}_1 + \mathrm{We}\,\overset{\triangledown}{\boldsymbol{\tau}}_1 = 2(1-\beta)\mathbf{D} + \mathrm{div}\left(\frac{\delta h_0}{|\mathbf{v}|^2}(\mathbf{v}\otimes\mathbf{v})\nabla\boldsymbol{\tau}_1\right). \tag{5.11b}$$

Here h_0 is mesh element size and δ is a parameter which scales the amount of artificial diffusion.

5.2.2 Weak formulation

The weak formulation of the problem with artificial diffusion reads

Find $(p, \mathbf{v}, \boldsymbol{\tau}_1) \in Q \times V \times S$ *such that*

$$\int_\Omega \mathrm{div}\,\mathbf{v} q\,\mathrm{d}\Omega = 0 \tag{5.12}$$

$$\int_\Omega \mathrm{Re}\,\dot{\mathbf{v}}\cdot\mathbf{u}\,\mathrm{d}\Omega = -\int_\Omega \mathbf{T}\cdot\nabla\mathbf{u} - \frac{\delta h_0}{|\mathbf{v}|^2}(\mathbf{v}\cdot\nabla\mathbf{v})\cdot(\mathbf{v}\cdot\nabla\mathbf{u})\,\mathrm{d}\Omega \tag{5.13}$$

$$\int_\Omega (\boldsymbol{\tau}_1 + \mathrm{We}\,\overset{\triangledown}{\boldsymbol{\tau}}_1)\cdot\mathbf{S}\,\mathrm{d}\Omega = \int_\Omega 2(1-\beta)\mathbf{D}\cdot\mathbf{S} - \frac{\delta h_0}{|\mathbf{v}|^2}(\mathbf{v}\cdot\nabla\boldsymbol{\tau}_1)\cdot(\mathbf{v}\cdot\nabla\mathbf{S})\,\mathrm{d}\Omega \tag{5.14}$$

for all $q \in Q$, $\mathbf{u} \in V_0$ *and* $\mathbf{S} \in S_0$.

5.2.3 Stream function

For postprocessing we need to know the stream function in the computational domain precisely. According to [18] we define ψ by

$$\frac{\partial \psi}{\partial x} = v_y, \qquad \frac{\partial \psi}{\partial y} = -v_x, \qquad \psi(0,0) = 1\,, \tag{5.15}$$

which implies

$$\Delta \psi = -\frac{\partial v_x}{\partial y} + \frac{\partial v_y}{\partial x}\,. \tag{5.16}$$

The boundary conditions for $\mathbf{v}$ together with $(5.15)_3$ imply that $\psi = 0$ on rigid walls, $\psi = 1$ on the axis of symmetry and $\frac{\partial \psi}{\partial x} = 0$ on both inlet and outlet. By solving the Poisson's equation (5.16) together with these boundary conditions we obtain the desired stream function. Since there is only a one way coupling between the equation for ψ (5.16) and the governing equations of the flow (5.3), we can solve (5.16) after we have solved (5.3) and thus the computation of ψ does not affect the computation of the flow at all.

5.3 Numerical results

Our simulations were performed on three different non-uniform meshes, which are refined near the re-entrant corner. They differ in the number of elements, their characteristics are summarized in Table 5.1 and the most refined Mesh 3 is shown in Figure 5.2. The computations were carried out for $\beta = 1/9$, $0 \leq \mathrm{Re} \leq 1$ and $0 \leq \mathrm{We} \leq 2$ and for various values of the streamline diffusion parameter δ. If not specified, the results presented below were obtained on Mesh 3 with the lowest value of δ for which convergence was achieved and no large oscillations of the solution in the vicinity of the re-entrant corner were observed. Besides the value of δ the success of the simulation depends to a large extent on the choice of initial solution. For this purpose we have utilised either the solution from the less refined mesh or with lower value of We .

Mesh	Number of elements	Number of dofs.	Max. aspect ratio
Mesh 1	720	21222	3.9
Mesh 2	1620	46950	3.9
Mesh 3	2880	82758	3.9

Table 5.1: Mesh characteristics.

Two numerical characteristics studied are the salient vortex length L_1 and its intensity $\psi_{\max}$. The vortex length is defined as the distance between the

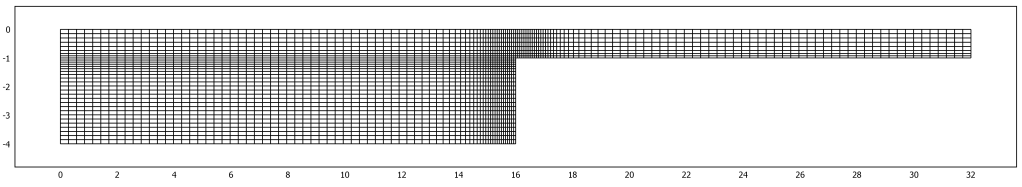

Figure 5.2: Mesh 3.

point, where the separation line meets the bottom of the channel and the salient corner (see Figure 5.1), the vortex intensity is the maximum of the stream function in the vortex. In Table 5.2 the vortex length and intensity are tabulated for different values of We along with the corresponding value of δ. For comparison, the values which have been obtained in [18] are shown in Table 5.3. In agreement with [18] the size of the vortex for $\mathrm{Re} = 1$ is approximately 20% smaller then for $\mathrm{Re} = 0$ and its intensity is smaller.

When $\mathrm{Re} = 0$ our results compare with [18] within an error of 10% for $\mathrm{We} \leq 1$. However, there is a qualitative difference: while according to our results the values of both L_1 and $\psi_{\max}$ slightly increase with increasing We, according to [18] they decrease between $\mathrm{We} = 0$ and $\mathrm{We} = 1$ and increase between $\mathrm{We} = 1.5$ and $\mathrm{We} = 2.5$. An explanation for this behavior might be the fact, that the value of δ has a significant impact on the solution. This is documented in Table 5.4, where corner vortex length and intensity are tabulated for different values of δ when $\mathrm{Re} = 0$ and $\mathrm{We} = 0.5$. It is evident that both L_1 and $\psi_{\max}$ increase with increasing δ.

When $\mathrm{Re} = 1$ the agreement is better, our results correspond to [18] within an error of 10% up to $\mathrm{We} = 1.5$ and the dependence on We exhibits the same behavior for all values of We.

The streamline patterns are presented in Figures 5.3 and 5.4 along with the streamlines taken from [18]. For $\mathrm{Re} = 0, \mathrm{We} < 1$ and $\mathrm{Re} = 1, \mathrm{We} = 0, 1$ they compare well to each other. According to [18], a lip vortex should appear for $\mathrm{Re} = 0, \mathrm{We} = 2$, which is not the case in our results. This is definitely due to the artificial diffusion, which smoothens such small structures in the solution.

In Figures 5.9 – 5.16 extra stress and pressure contours are plotted for $0 \leq \mathrm{Re} \leq 1$ and $0 \leq \mathrm{We} \leq 1$. All these contours are smooth and the development of extra stress boundary layer in the downstream channel is evident. The contours in Figures 5.13 and 5.14 are comparable with Figs. 11 and 12 in [18] respectively.

Pressure and the components of velocity and extra stress are plotted along the cross-section $y = -1$ for $0 \leq \mathrm{Re} \leq 1$, $0 \leq \mathrm{We} \leq 2$ in Figures 5.5 – 5.8. The extra stress cross-sections exhibit qualitatively the same behavior as the

			Mesh 1		Mesh 2		Mesh 3	
Re	We	δ	L_1	$\psi_{\max}$	L_1	$\psi_{\max}$	L_1	$\psi_{\max}$
0	0.0	0	1.432	1.00117	1.456	1.00117	1.467	1.00117
0	0.5	0.25	1.479	1.00138	1.479	1.00129	1.479	1.00124
0	1.0	0.5	1.560	1.00189	1.525	1.00156	1.505	1.00140
0	1.5	1.25	1.787	1.00384	1.694	1.00282	1.656	1.00245
0	2.0	2	1.978	1.00616	1.850	1.00450	1.763	1.00355
1	0.0	0	1.133	1.00043	1.162	1.00043	1.174	1.00043
1	0.5	0.25	1.110	1.00041	1.116	1.00037	1.113	1.00036
1	1.0	0.5	1.128	1.00046	1.099	1.00037	1.081	1.00033
1	1.5	1.25	1.328	1.00101	1.226	1.00064	1.162	1.00048
1	2.0	2	1.522	1.00199	1.363	1.00115	1.261	1.00077

Table 5.2: Dependence of L_1 and $\psi_{\max}$ on We and Re.

	Re $= 0$		Re $= 1$	
We	L_1	$\psi_{\max}$	L_1	$\psi_{\max}$
0.0	1.417	1.00118	1.164	1.00050
0.5	1.400	1.00114	1.093	1.00041
1.0	1.384	1.00110	1.048	1.00031
1.5	1.374	1.00110	1.013	1.00031
2.0	1.377	1.00118	0.986	1.00029

Table 5.3: Dependence of L_1 and $\psi_{\max}$ on We according to [18].

results plotted in Figs. 13 and 18 in [18] for both values of Re and We ≤ 1.5. For We > 1.5 there is a significant difference which is again due to artificial diffusion added to our equations.

To summarize, we have performed calculations of the flow of an Oldroyd-B fluid through a 4:1 planar contraction for Re $= 0, 1$, We $= 0, 0.5, 1, 1.5, 2$ and $\beta = 1/9$. Our results correspond well to the results obtained by [18] for We ≤ 1 when Re $= 0$ and We ≤ 1.5 when Re $= 1$. For higher values of We a significant departure from the results of [18] has been observed, which is in the first place due to the high amount of artificial diffusion added to the system to ensure convergence and in the second place due to insufficient resolution of the mesh near the re-entrant corner.

	Re $= 0$		Re $= 1$	
δ	L_1	$\psi_{\max}$	L_1	$\psi_{\max}$
0.00	1.421	1.00101	1.067	1.00030
0.25	1.479	1.00124	1.113	1.00036
0.50	1.511	1.00138	1.148	1.00041
0.75	1.534	1.00150	1.177	1.00046
1.00	1.554	1.00161	1.200	1.00050

Table 5.4: Dependence of L_1 and $\psi_{\max}$ on δ when We $= 0.5$.

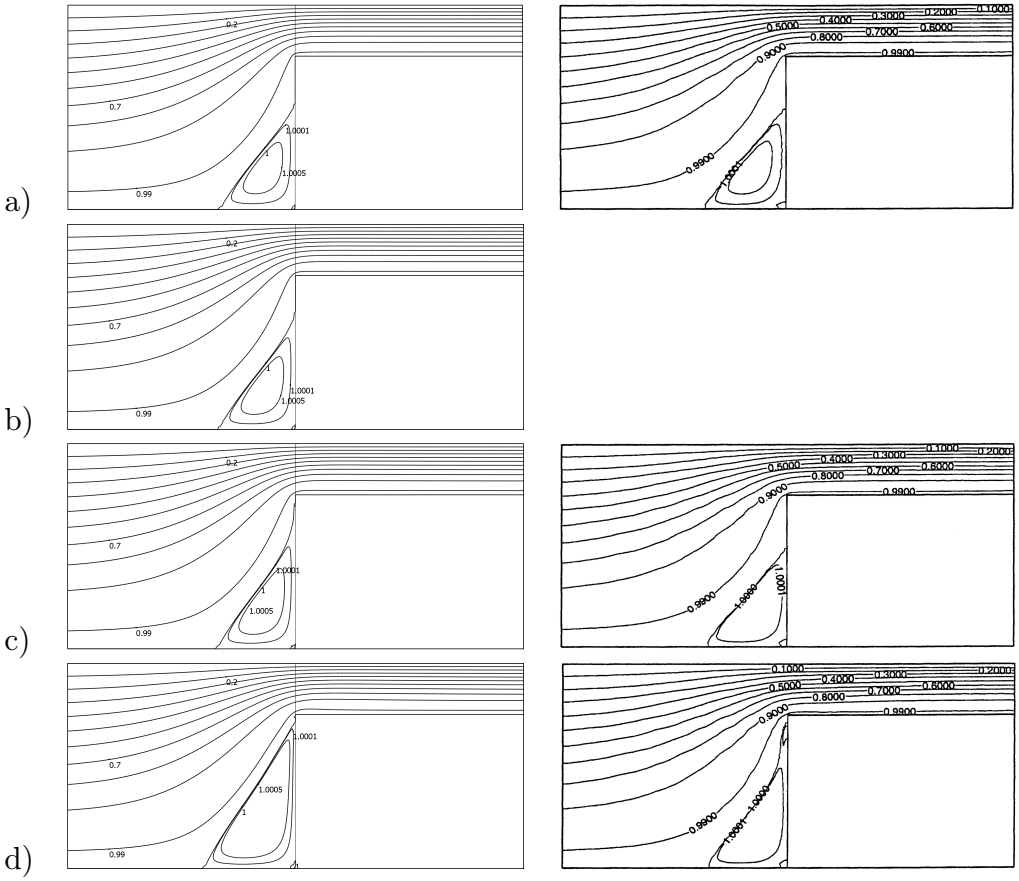

Figure 5.3: The streamlines for (a) We $= 0$ (b) We $= 0.5$ (c) We $= 1$ (d) We $= 2$ when Re $= 0$. Left according to our computation, right according to [18] (if available).

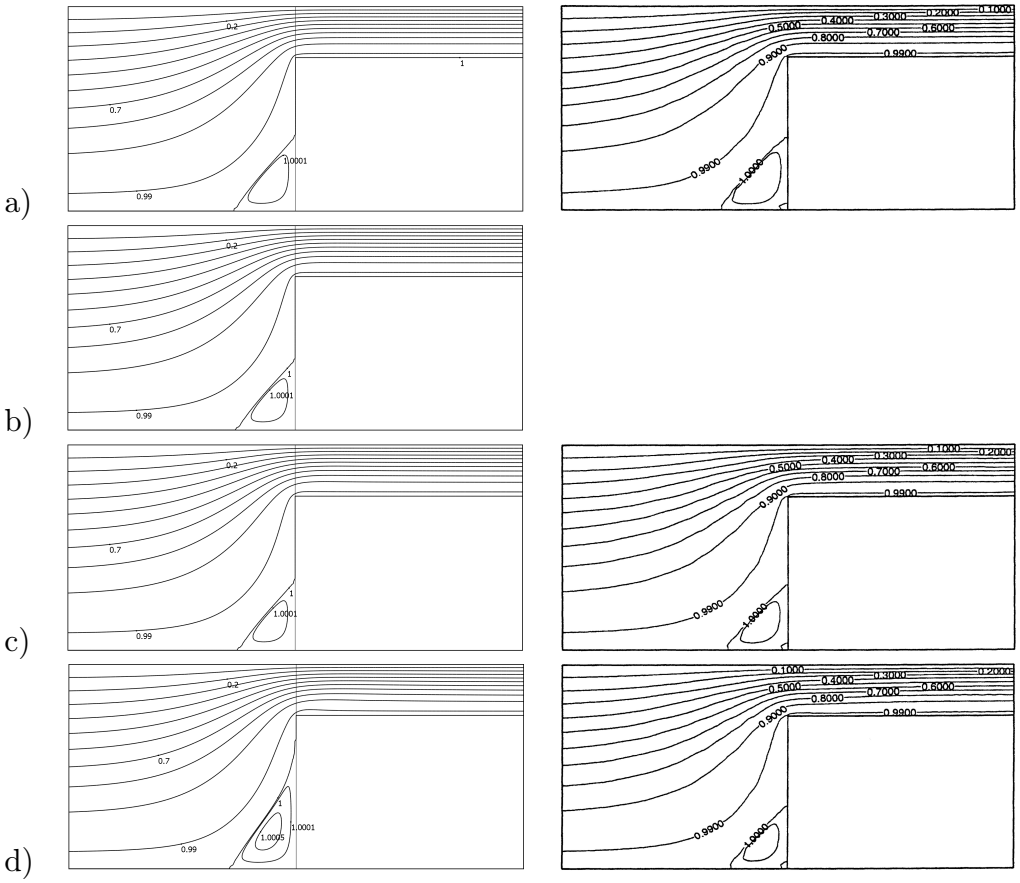

Figure 5.4: The streamlines for (a) We = 0 (b) We = 0.5 (c) We = 1 (d) We = 2 when Re = 1. Left according to our computation, right according to [18] (if available).

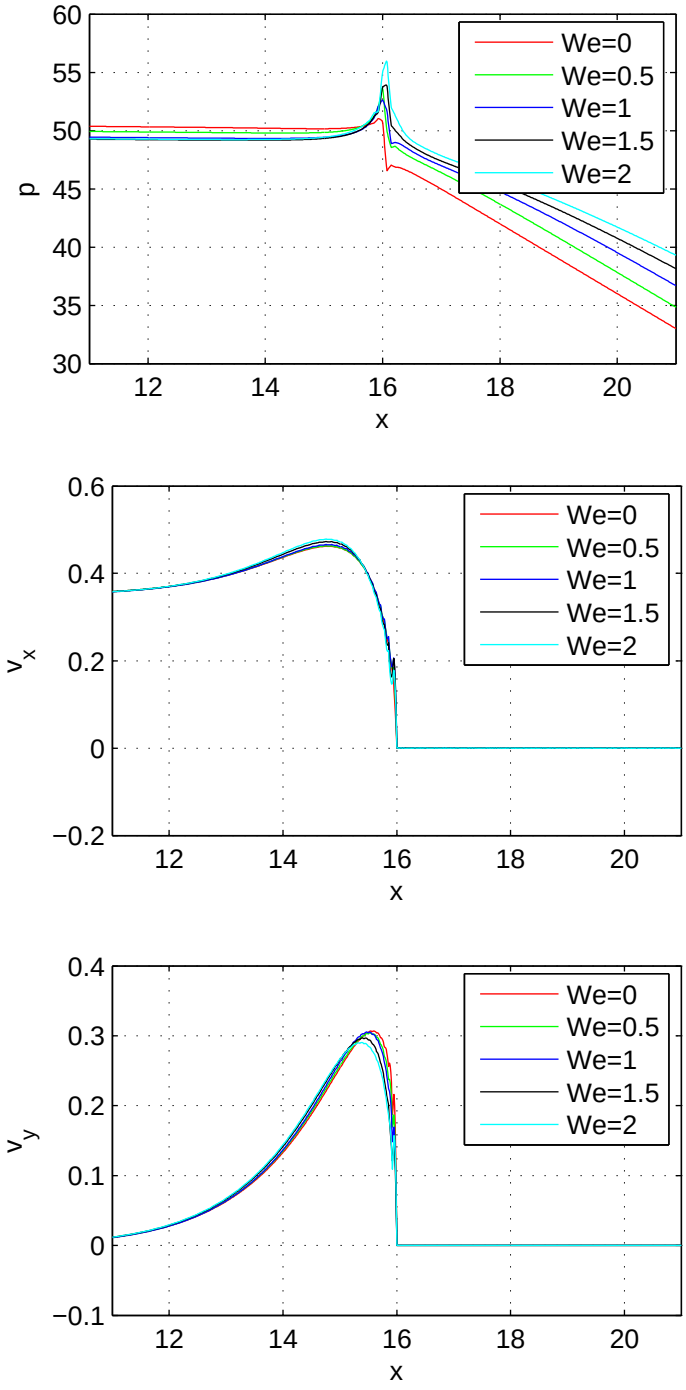

Figure 5.5: The values of p, v_x and v_y along $y = -1$ when $\mathrm{Re} = 0$.

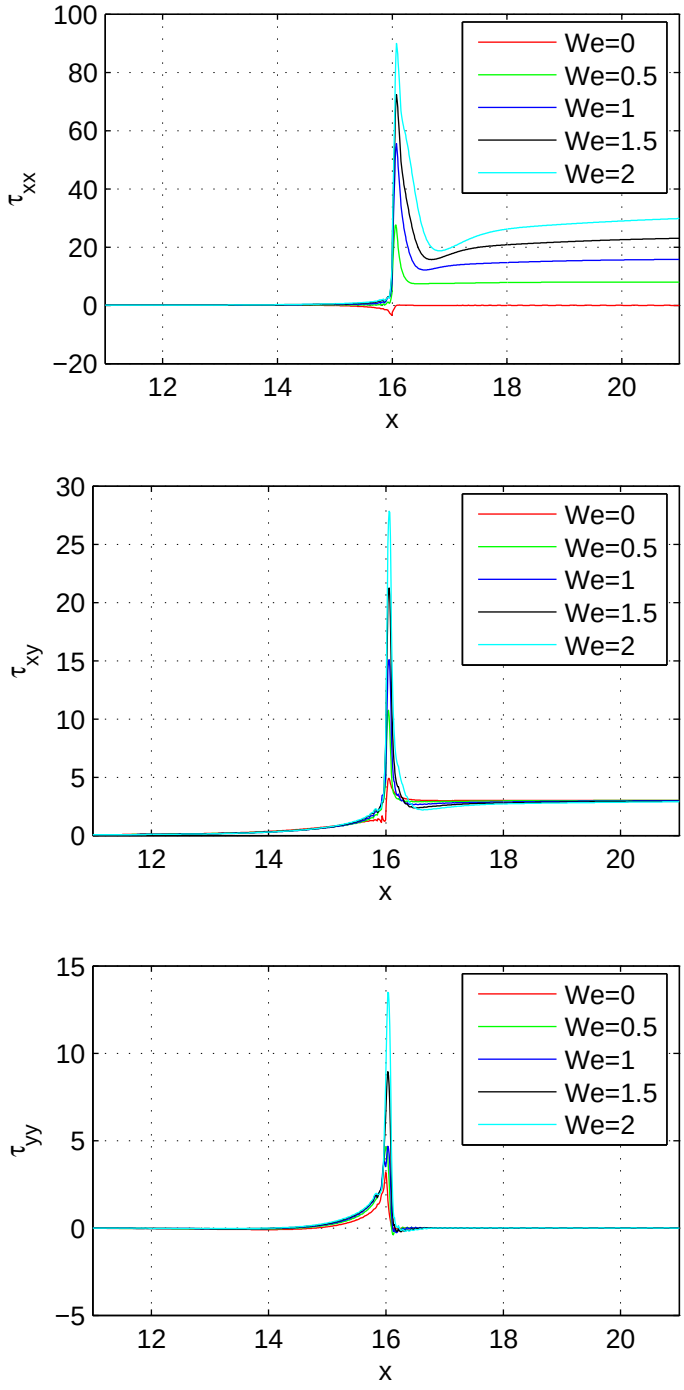

Figure 5.6: The values of τ_{xx}, τ_{xy} and τ_{yy} along $y = -1$ when $\mathrm{Re} = 0$.

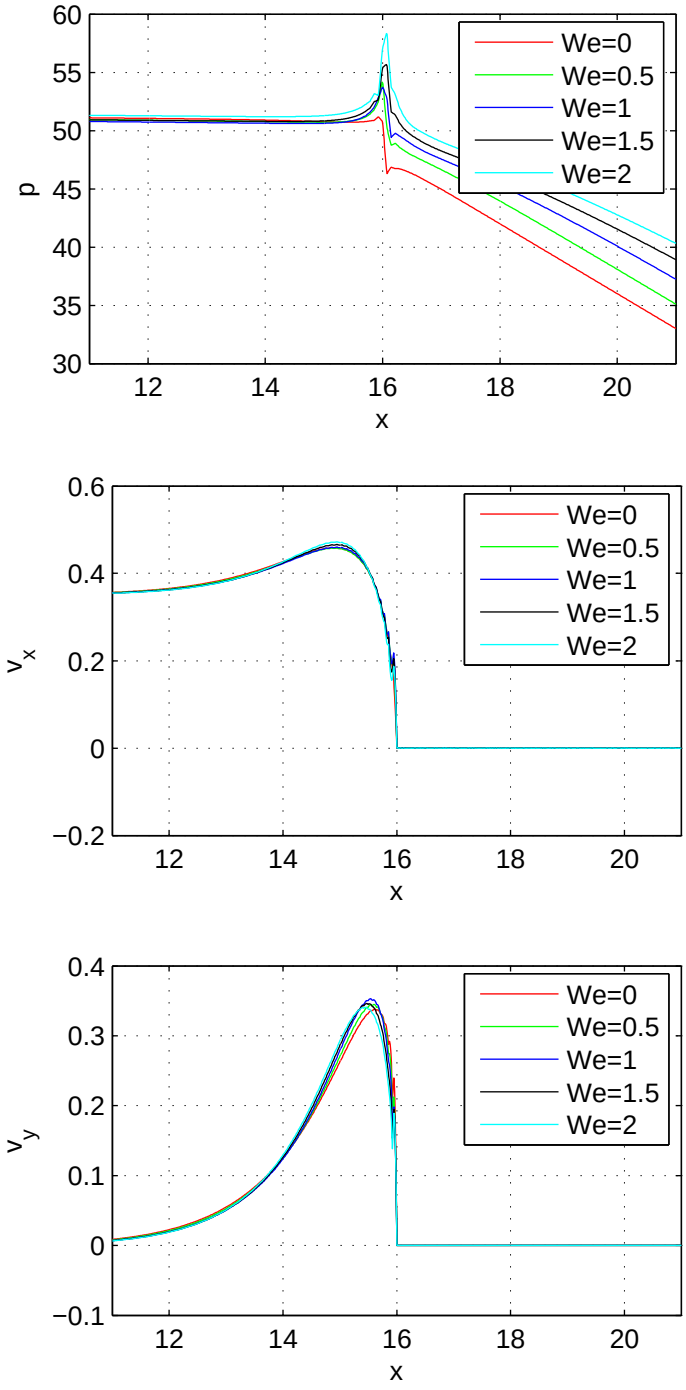

Figure 5.7: The values of p, v_x and v_y along $y = -1$ when $\mathrm{Re} = 1$.

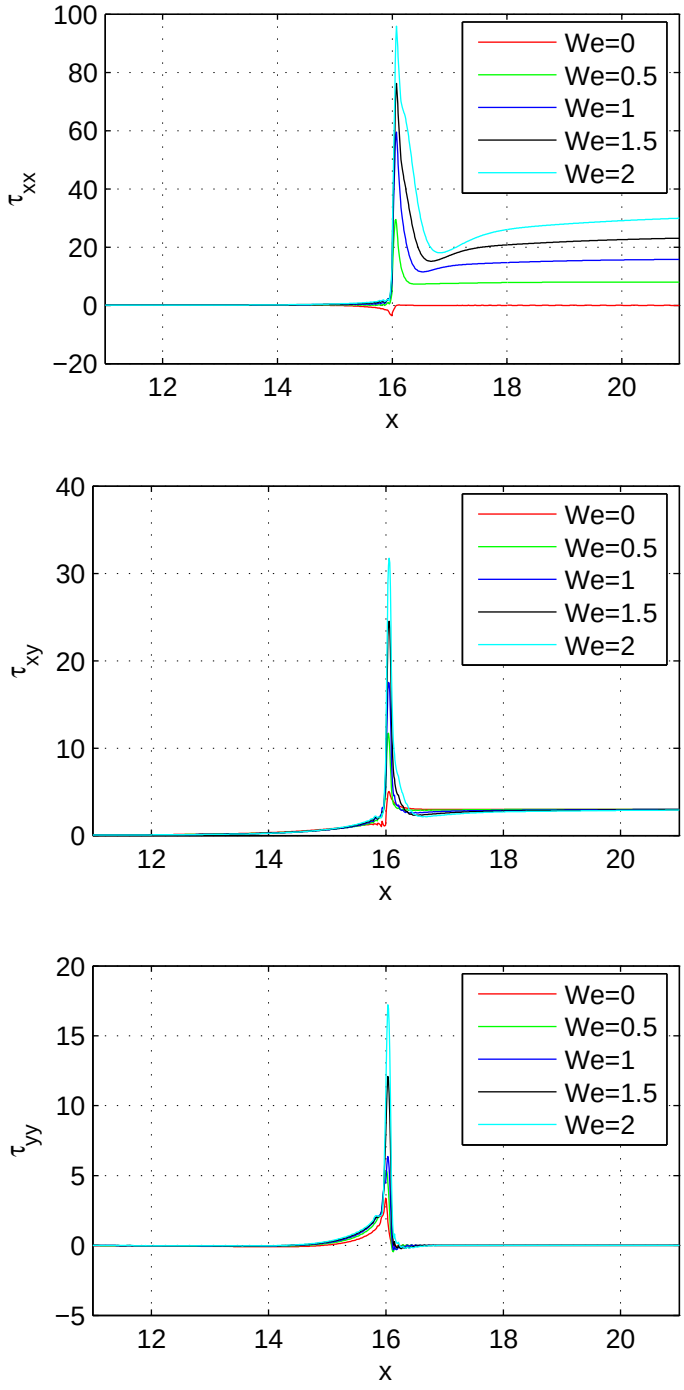

Figure 5.8: The values of τ_{xx}, τ_{xy} and τ_{yy} along $y = -1$ when $\mathrm{Re} = 1$.

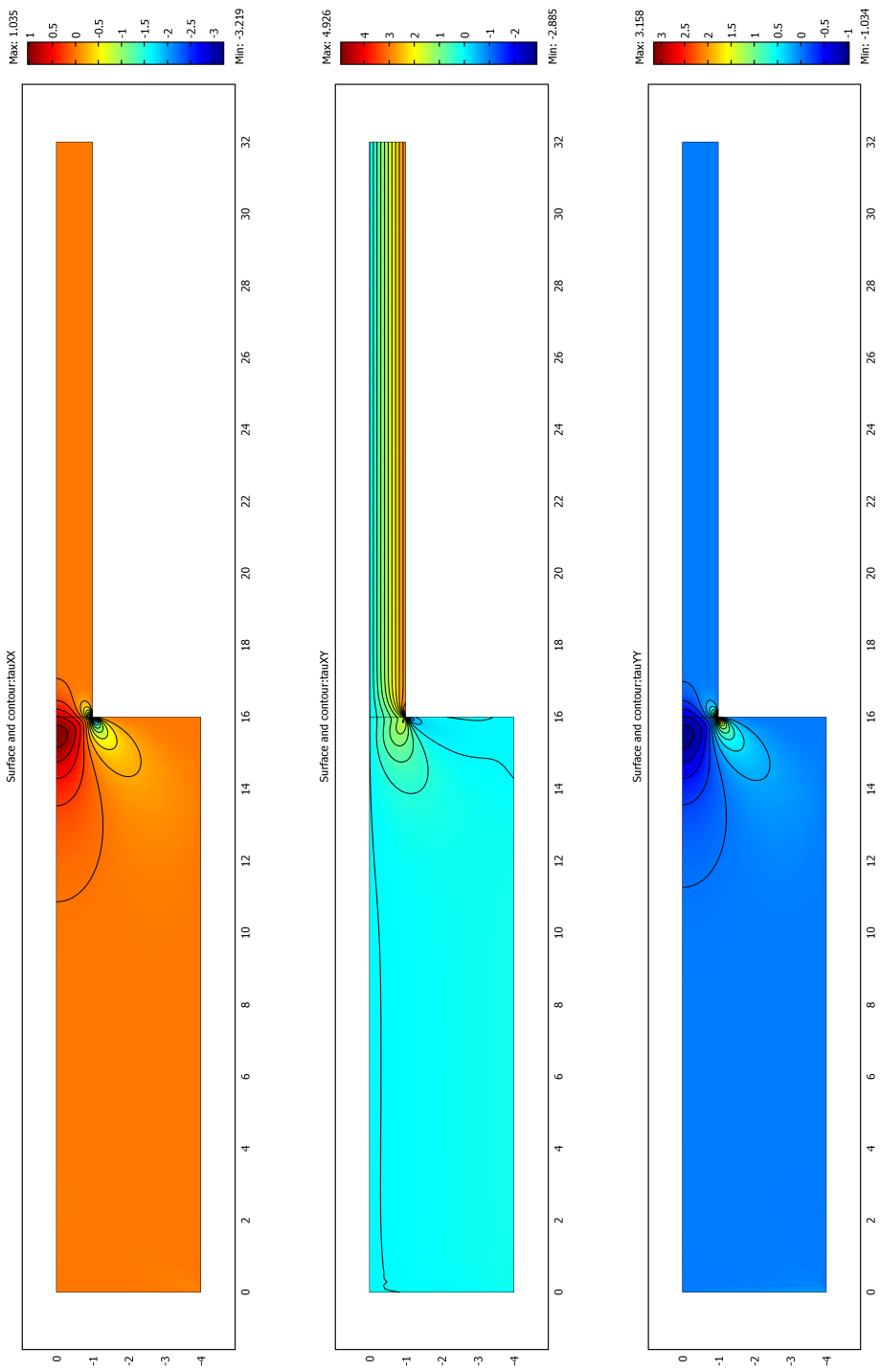

Figure 5.9: The stress contours for (a) τ_{xx}, (b) τ_{xy} and (c) τ_{yy} for We $= 0$ and Re $= 0$.

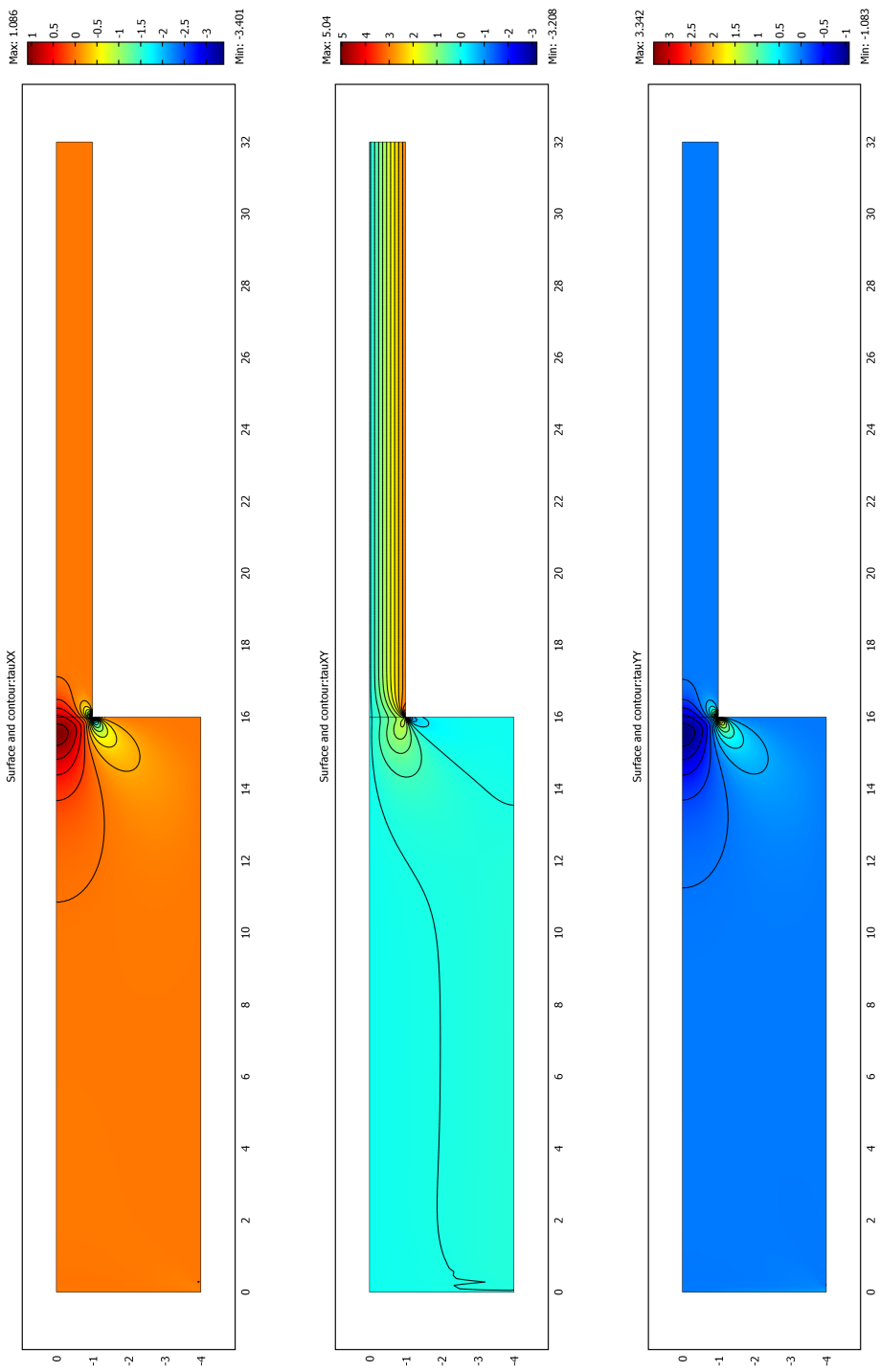

Figure 5.10: The stress contours for (a) τ_{xx}, (b) τ_{xy} and (c) τ_{yy} for We $= 0$ and Re $= 1$.

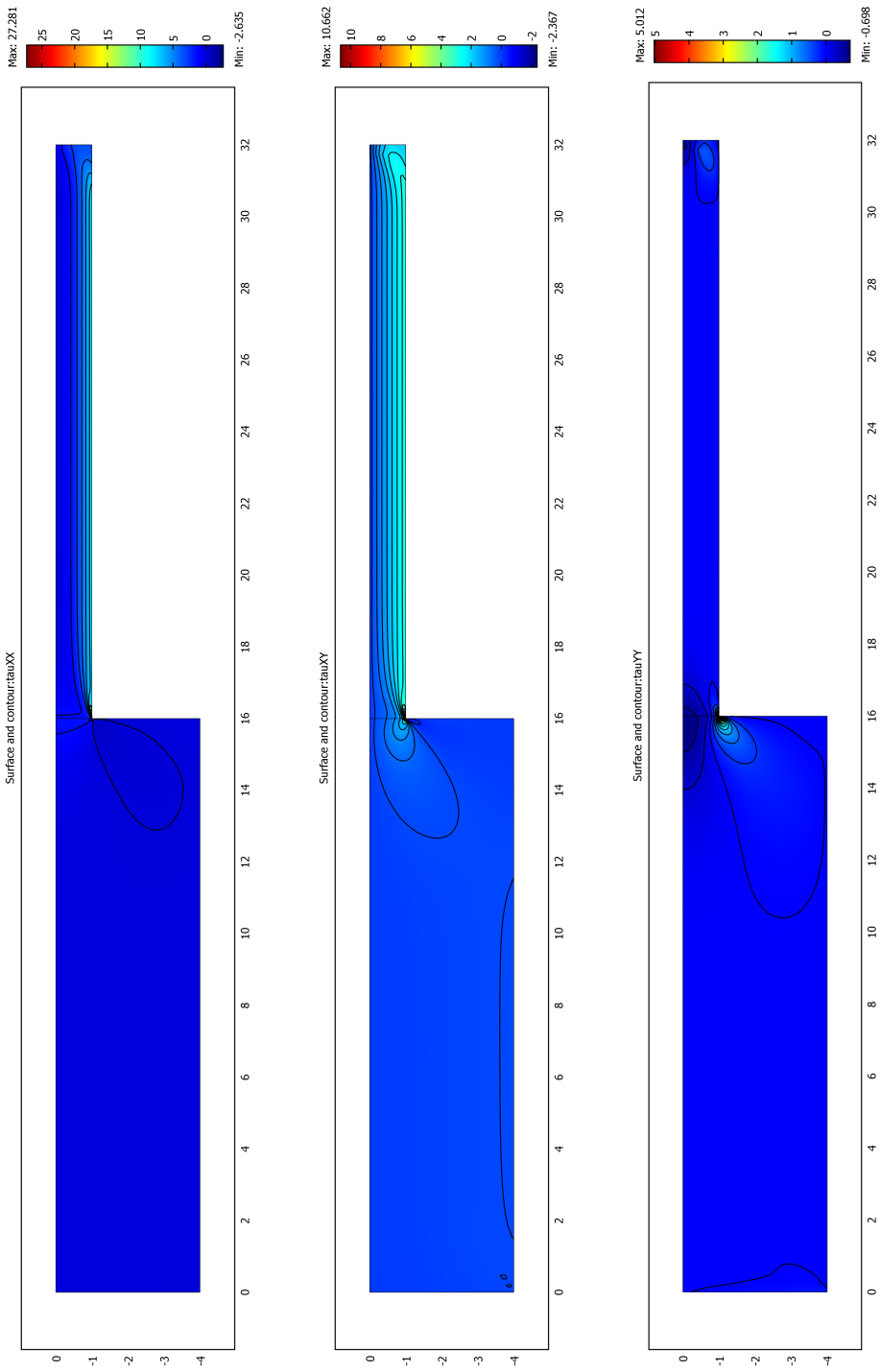

Figure 5.11: The stress contours for (a) τ_{xx}, (b) τ_{xy} and (c) τ_{yy} for We $= 0.5$ and Re $= 0$.

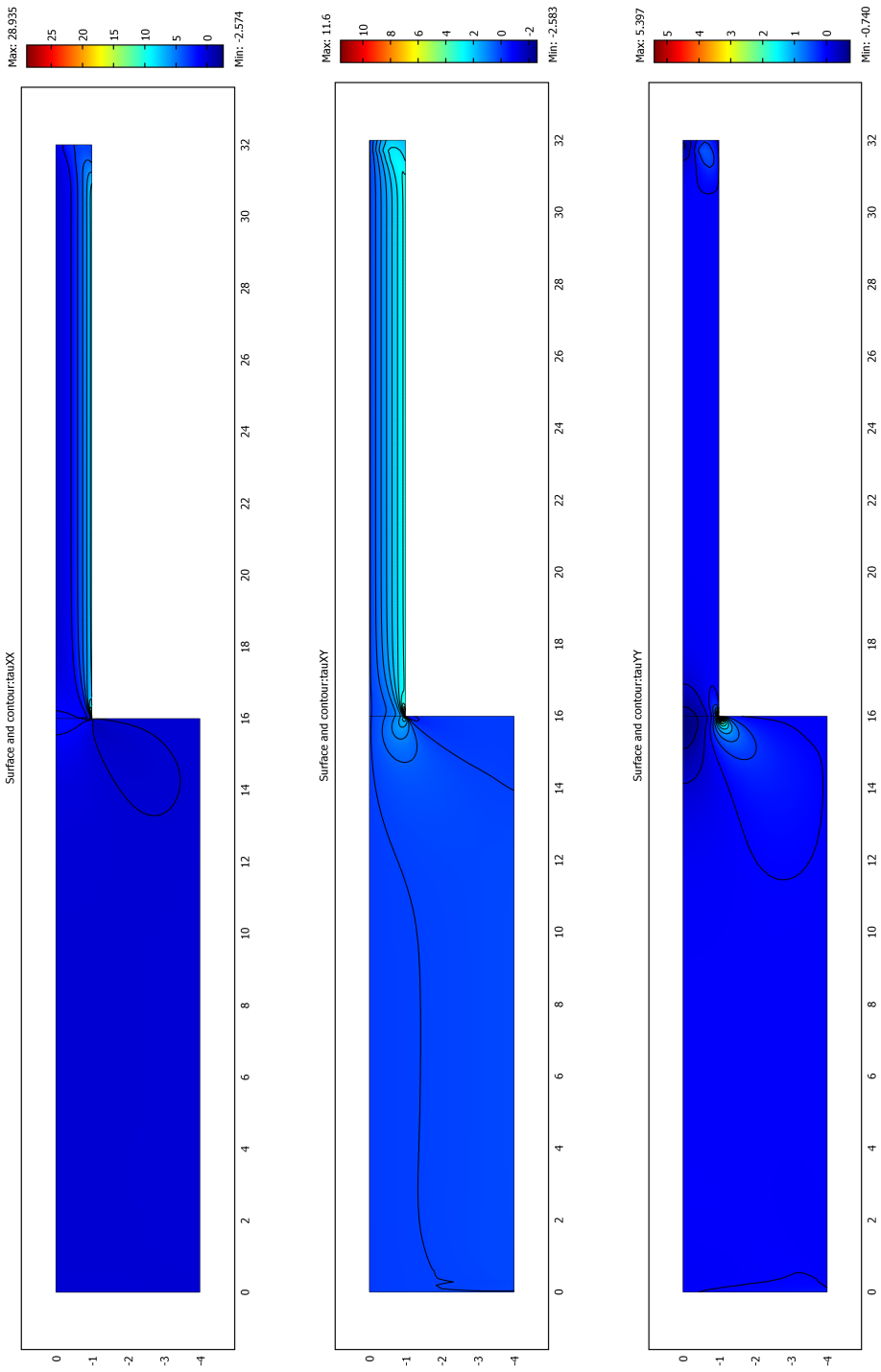

Figure 5.12: The stress contours for (a) τ_{xx}, (b) τ_{xy} and (c) τ_{yy} for We $= 0.5$ and Re $= 1$.

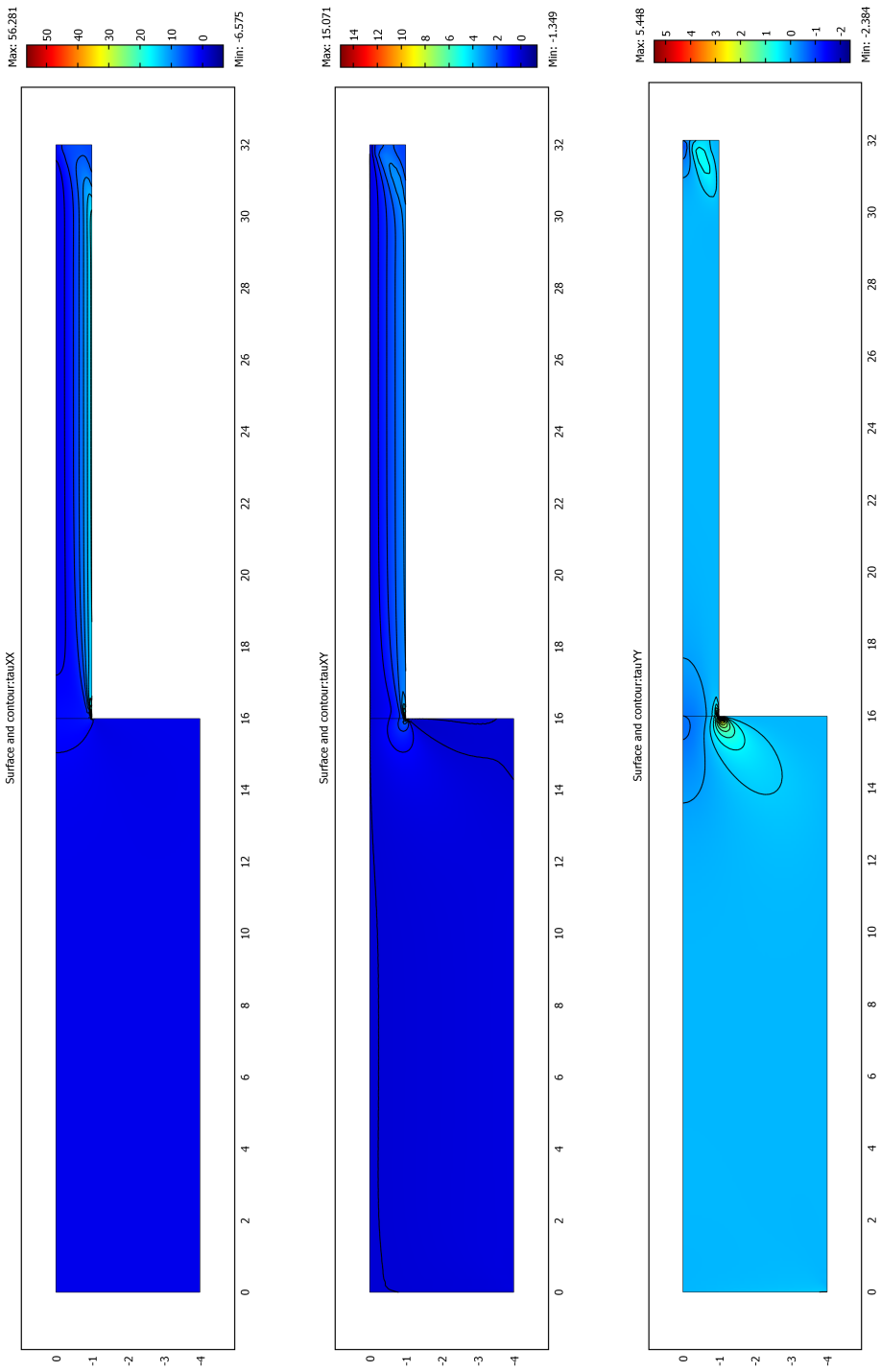

Figure 5.13: The stress contours for (a) τ_{xx}, (b) τ_{xy} and (c) τ_{yy} for We $= 1$ and Re $= 0$.

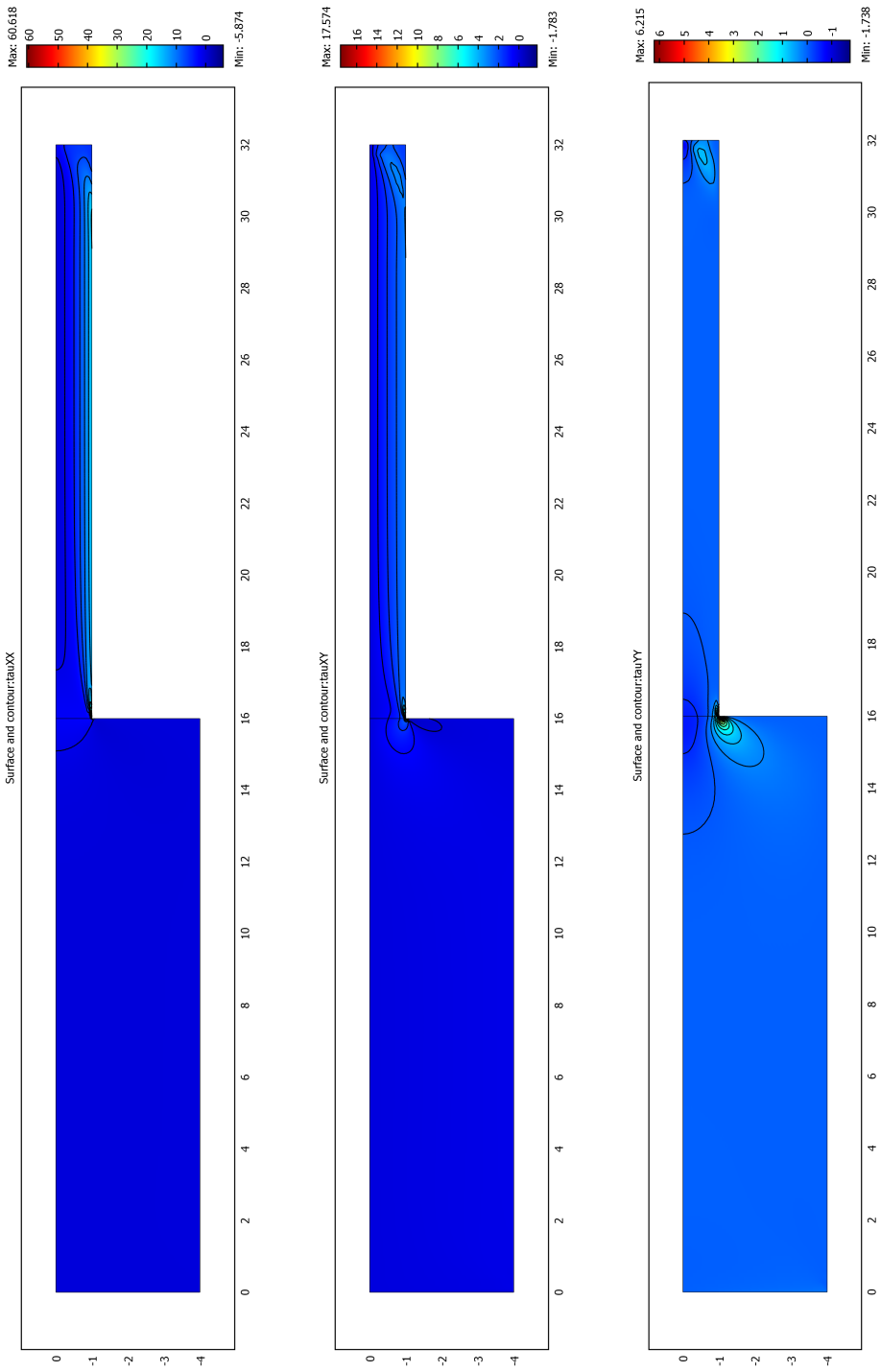

Figure 5.14: The stress contours for (a) τ_{xx}, (b) τ_{xy} and (c) τ_{yy} for We $= 1$ and Re $= 1$.

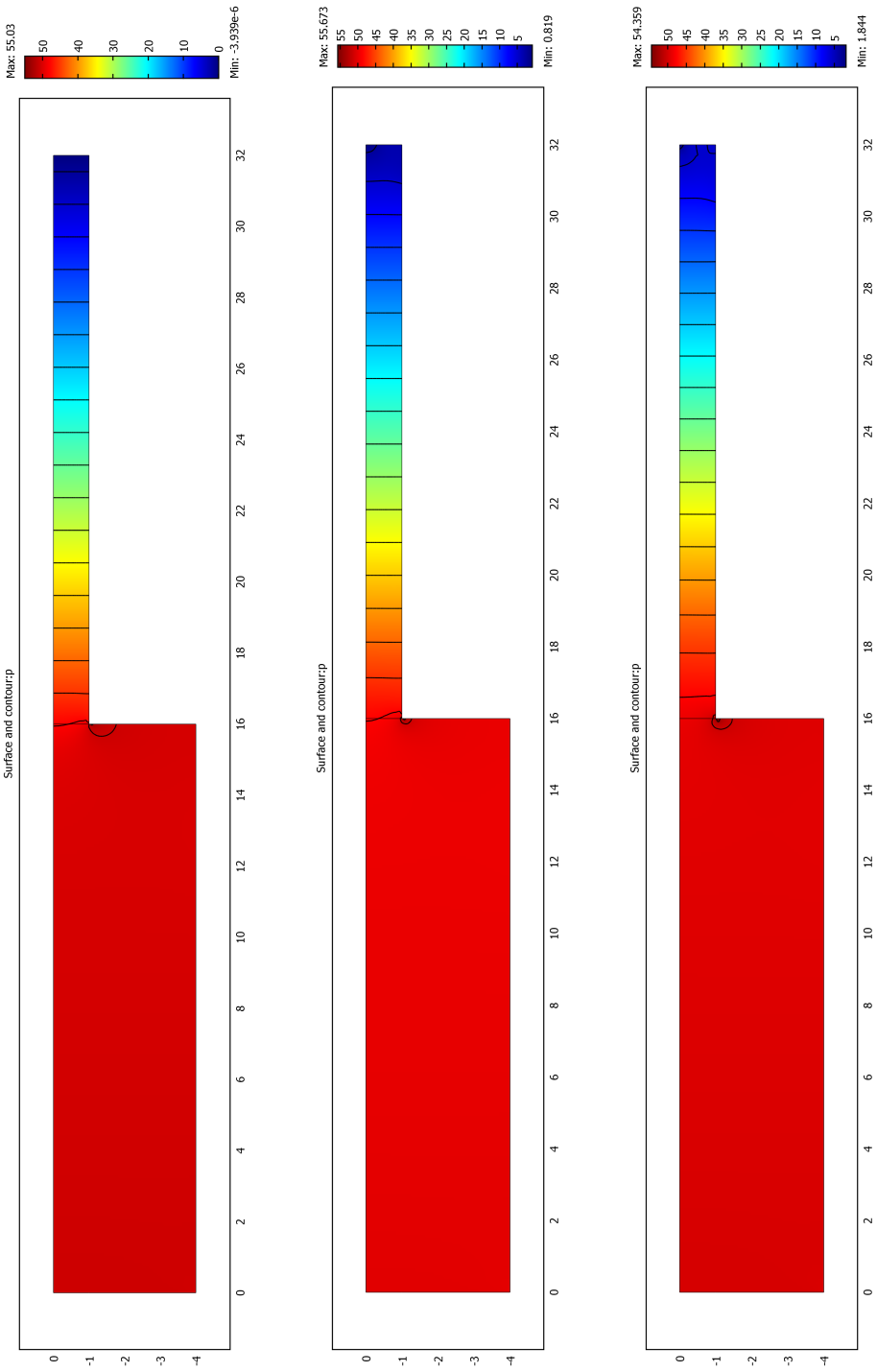

Figure 5.15: The pressure contours for (a) We = 0 (b) We = 0.5 (c) We = 1 when Re = 0.

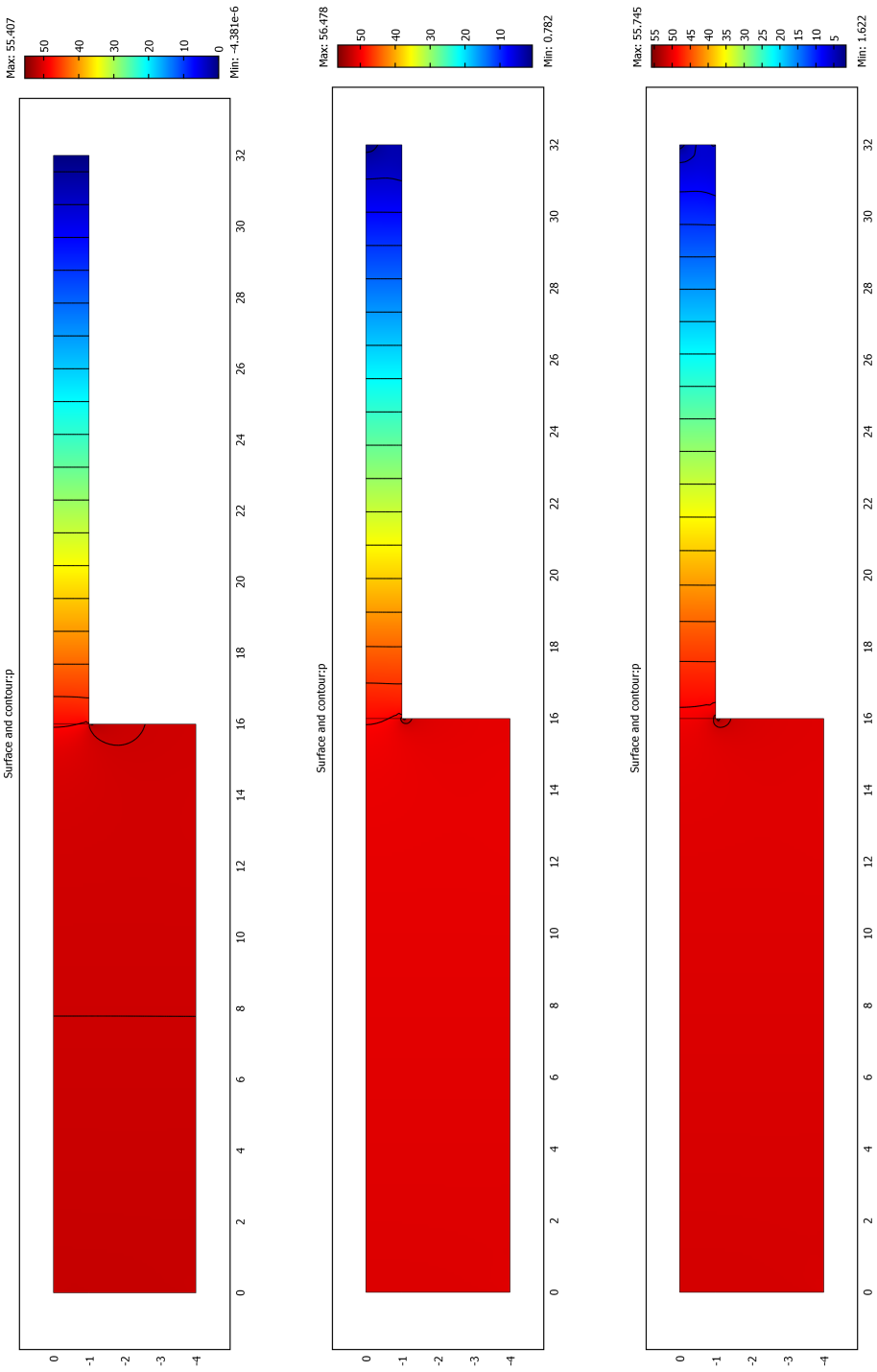

Figure 5.16: The pressure contours for (a) We = 0 (b) We = 0.5 (c) We = 1 when Re = 1.

Chapter 6

Axially symmetric cylinder flow

Our last problem is the axially symmetric flow in a cylinder. Firstly, we discuss the behavior of the Newtonian fluid at the given geometry. Secondly, we solve the equations for Oldroyd-B and Model 1 under certain simplifications and fit the experimental data with the results. Finally, we solve the equations without any simplifications, assuming only that the flow is axially symmetric.

6.1 Problem description

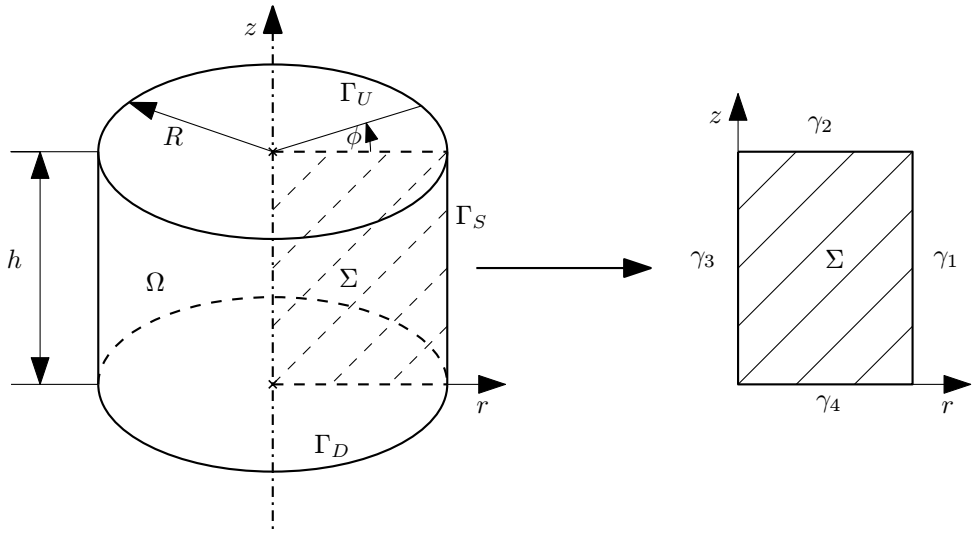

Figure 6.1: The geometry of axially symmetric flow in a cylinder.

For the description of the flow we employ cylindrical coordinates r, ϕ, z with standard physical basis $\mathbf{e}_r$, $\mathbf{e}_\phi$, $\mathbf{e}_z$ (i.e., the norm of these vectors is one), all components of tensors will be given with respect to this basis.

The geometry shown in Figure 6.1 comprises a cylinder of radius R and height h. Its bottom is at rest while the top is rotating as a rigid body with a given angular velocity, which is either a constant or a step function of time $\omega(t) = \omega H(t)$. The boundary on the sides of the cylinder is free which allows the fluid to enter and leave the cylinder. However, this is not a problem because the inflow and outflow are either zero or negligible in the given experiment. Thus, the considered conditions on the boundary of the cylinder are

$$\mathbf{v} = 0 \text{ on } \Gamma_D \tag{6.1a}$$
$$\mathbf{v} = \omega r \mathbf{e}_\phi \text{ on } \Gamma_U \tag{6.1b}$$
$$\mathbf{T}\mathbf{n} = 0 \text{ on } \Gamma_S\,. \tag{6.1c}$$

As for the initial conditions, we assume that the material is at rest and relaxed when the experiment starts, which means

$$\mathbf{v}(0,\mathbf{x}) = 0 \tag{6.2a}$$
$$\mathbf{A}(0,\mathbf{x}) = 0 \text{ for Oldroyd-B} \tag{6.2b}$$
$$\mathbf{B}^{\delta}_{\kappa_p}(0,\mathbf{x}) = 0 \text{ and } b(0,\mathbf{x}) = 3 \text{ for Model 1}\ . \tag{6.2c}$$

The most important assumption made in this example is that the flow is axially symmetric, i.e. neither pressure nor any of the components of velocity and extra-stress depends on the angle ϕ. This allows us to reduce the computational domain to the 2D cross-section Σ (see Figure 6.1) and thus noticeably reduce the size of the problem.

We are mainly interested in determining the relevant torque given by the formula

$$M = \int_{\Gamma_U} r T_{\phi z}\,\mathrm{d}S\,, \tag{6.3}$$

that in the case of axial symmetry takes the form

$$M = \int_0^R 2\pi r^2 T_{\phi z}(r,h)\,\mathrm{d}r\,. \tag{6.4}$$

6.2 Newtonian fluid

In order to understand some of the problems arising from the cylindrical geometry, we first investigate the flow of a Newtonian fluid governed by the Navier-Stokes equations in the above described situation.

6.2.1 Steady flow

If we neglect the convective term (i.e. if we consider the Stokes instead of the Navier-Stokes equations), then the above described problem has a simple analytical solution

$$p = 0 \tag{6.5}$$

$$\mathbf{v} = \frac{\omega r z}{h}\mathbf{e}_\phi\,, \tag{6.6}$$

i.e. the velocity is perpendicular to the axis and thus has no component in the rz plane. Unfortunately, without neglecting the convective term the Navier-Stokes equations do not posses a similar analytical solution in the form $\mathbf{v} = v_\phi(r,z)\mathbf{e}_\phi$, which can be easily shown in the following way. The Navier–Stokes equations with this ansatz read

$$-\varrho\frac{v_\phi^2}{r} = -\frac{\partial p}{\partial r} \tag{6.7}$$

$$0 = -\frac{1}{r}\frac{\partial p}{\partial \phi} + \eta\left(\frac{\partial^2 v_\phi}{\partial r^2} + \frac{1}{r}\frac{\partial v_\phi}{\partial r} - \frac{v_\phi}{r^2} + \frac{\partial^2 v_\phi}{\partial z^2}\right) \tag{6.8}$$

$$0 = -\frac{\partial p}{\partial z}. \tag{6.9}$$

The integrability condition for pressure

$$\frac{\partial^2 p}{\partial r \partial z} = \frac{\partial^2 p}{\partial z \partial r} \tag{6.10}$$

leads to

$$0 = \frac{\partial}{\partial z}\varrho\frac{v_\phi^2}{r} \tag{6.11}$$

which implies that

$$0 = v_\phi\frac{\partial v_\phi}{\partial z} = \frac{\partial}{\partial z}\frac{v_\phi^2}{2}\,. \tag{6.12}$$

This condition could be fulfilled only if the angular velocity v_ϕ on the top of the cylinder was equal to the angular velocity on the bottom. Since this is not the case, we have to reject the assumption $\mathbf{v} = v_\phi(r,z)\mathbf{e}_\phi$ and assume that all the components of $\mathbf{v}$ are generally nonzero. Numerical solution of the Navier-Stokes equations at the given geometry reveal that besides the primary flow perpendicular to the axis a secondary flow in the rz plane arises. This secondary flow, which is caused by the inertial forces, is shown in Figure 6.2 below.

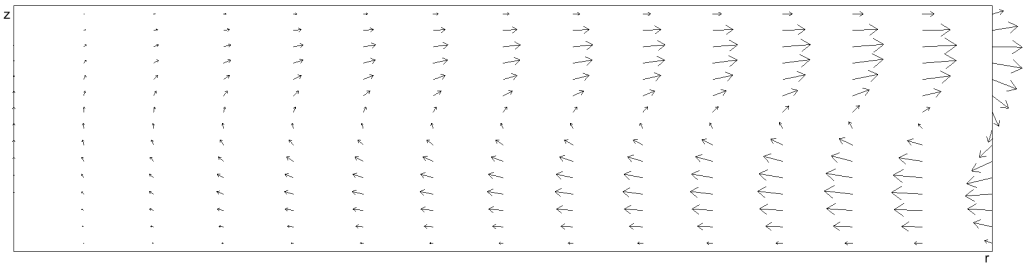

Figure 6.2: Secondary flow pattern in the rz plane for small Re .

6.2.2 Unsteady flow

Further difficulties arise in the case of an unsteady flow i.e. when ω is not constant. If we substitute the ansatz

$$\mathbf{v} = \frac{\omega(t) r z}{h} \mathbf{e}_\phi \tag{6.13}$$

into the Stokes equations, we obtain $\frac{\mathrm{d}\omega}{\mathrm{d}t} = 0$, which is clearly a contradiction. However, analytical solution of the flow with $\omega(t) = \omega H(t)$ using Fourier series reveals that the time in which the velocity profile (6.13) establishes is of the order

$$\tau_0 \approx \frac{\rho(R^2 + h^2)}{\eta}\,, \tag{6.14}$$

which is approximately $10^{-8}\,\mathrm{s}$ and thus negligible in the considered experiment.

6.3 Solution under simplifying assumption

In order to investigate only the important features of the flow, we would like to simplify its governing equations as much as possible. Motivated by the discussion of the Newtonian flow, we firstly neglect the convective term. This simplification is well justified, because the Reynolds number

$$\mathrm{Re} = \frac{\rho \omega R L}{\eta} \tag{6.15}$$

is of the order 10^{-7} in the considered experiment. We will show that under this assumption the equations describing the steady flow of both Oldroyd-B and Model 1 fluids have an analytical solution, where the velocity is given by

$$\mathbf{v} = \frac{\omega r z}{h} \mathbf{e}_\phi\,. \tag{6.16}$$

As for the unsteady flow driven by $\omega(t) = \omega H(t)$, the velocity profile of the form (6.16) is not possible because after the upper plate was set to motion it takes some time before the fluid starts to rotate in the whole cylinder. However, the characteristic time of this transient effect is several orders of magnitude lower that the viscoelastic relaxation time and numerical solution without any simplifications discussed in Section 6.5 reveal, that this effect does not have any influence on the further development of the flow. Therefore, we will assume the velocity to be given by

$$\mathbf{v} = \frac{\omega(t) r z}{h} \mathbf{e}_\phi \tag{6.17}$$

and neglect the term $\frac{\mathrm{d}\omega}{\mathrm{d}t}$ throughout this section. This basically means that we neglect the material time derivative of velocity, while we keep the material time derivative of elastic stress, which might be thought of as a kind of 'quasi-static' approximation.

6.3.1 Oldroyd-B

Steady flow

In the steady state the governing equations of Oldroyd-B (2.11) with the ansatz

$$p = p(r, z), \quad \mathbf{v} = \frac{\omega r z}{h} \mathbf{e}_\phi \tag{6.18}$$

$$\mathbf{A} = \begin{pmatrix} A_{rr}(r,z) & A_{r\phi}(r,z) & A_{rz}(r,z) \\ A_{r\phi}(r,z) & A_{\phi\phi}(r,z) & A_{\phi z}(r,z) \\ A_{rz}(r,z) & A_{\phi z}(r,z) & A_{zz}(r,z) \end{pmatrix} \tag{6.19}$$

and under the neglect of the convective term take the form

$$0 = -\frac{\partial p}{\partial r} + G\left(\frac{\partial A_{rr}}{\partial r} + \frac{A_{rr}}{r} - \frac{A_{\phi\phi}}{r} + \frac{\partial A_{rz}}{\partial z}\right) \tag{6.20a}$$

$$0 = G\left(\frac{\partial A_{r\phi}}{\partial r} + \frac{2A_{r\phi}}{r} + \frac{\partial A_{\phi z}}{\partial z}\right) \tag{6.20b}$$

$$0 = -\frac{\partial p}{\partial z} + G\left(\frac{\partial A_{rz}}{\partial r} + \frac{A_{rz}}{r} + \frac{\partial A_{zz}}{\partial z}\right) \tag{6.20c}$$

$$A_{rr} = 0 \tag{6.20d}$$

$$A_{r\phi} - \frac{\tau r \omega}{h} A_{rz} = 0 \tag{6.20e}$$

$$A_{rz} = 0 \tag{6.20f}$$

$$A_{\phi\phi} - \frac{2\tau r \omega}{h} A_{\phi z} = 0 \tag{6.20g}$$

$$A_{\phi z} - \frac{\tau r\omega}{h} A_{zz} = \frac{\tau r\omega}{h} \tag{6.20h}$$

$$A_{zz} = 0\,. \tag{6.20i}$$

It can be easily checked that these equations together with the boundary conditions (6.1) have a simple analytical solution

$$p = G\left(\frac{\tau\omega}{h}\right)^2 \left(R^2 - r^2\right) \tag{6.21}$$

$$A_{rr} = A_{r\phi} = A_{rz} = A_{zz} = 0 \tag{6.22}$$

$$A_{\phi\phi} = 2\left(\frac{\tau r\omega}{h}\right)^2 \tag{6.23}$$

$$A_{\phi z} = \frac{\tau r\omega}{h}\,. \tag{6.24}$$

Unsteady flow

In the case of an unsteady flow the governing equations of Oldroyd-B (2.11) with the ansatz

$$p = p(t, r, z), \quad \mathbf{v} = \frac{\omega(t) r z}{h}\mathbf{e}_\phi \tag{6.25}$$

$$\mathbf{A} = \begin{pmatrix} A_{rr}(t,r,z) & A_{r\phi}(t,r,z) & A_{rz}(t,r,z) \\ A_{r\phi}(t,r,z) & A_{\phi\phi}(t,r,z) & A_{\phi z}(t,r,z) \\ A_{rz}(t,r,z) & A_{\phi z}(t,r,z) & A_{zz}(t,r,z) \end{pmatrix} \tag{6.26}$$

and under the neglect of the convective term take the form

$$0 = -\frac{\partial p}{\partial r} + G\left(\frac{\partial A_{rr}}{\partial r} + \frac{A_{rr}}{r} - \frac{A_{\phi\phi}}{r} + \frac{\partial A_{rz}}{\partial z}\right) \tag{6.27a}$$

$$\rho\frac{rz}{h}\frac{\mathrm{d}\omega}{\mathrm{d}t} = G\left(\frac{\partial A_{r\phi}}{\partial r} + \frac{2A_{r\phi}}{r} + \frac{\partial A_{\phi z}}{\partial z}\right) \tag{6.27b}$$

$$0 = -\frac{\partial p}{\partial z} + G\left(\frac{\partial A_{rz}}{\partial r} + \frac{A_{rz}}{r} + \frac{\partial A_{zz}}{\partial z}\right) \tag{6.27c}$$

$$A_{rr} + \tau\frac{\partial A_{rr}}{\partial t} = 0 \tag{6.27d}$$

$$A_{r\phi} + \tau\left(\frac{\partial A_{r\phi}}{\partial t} - \frac{r\omega}{h}A_{rz}\right) = 0 \tag{6.27e}$$

$$A_{rz} + \tau\frac{\partial A_{rz}}{\partial t} = 0 \tag{6.27f}$$

$$A_{\phi\phi} + \tau\left(\frac{\partial A_{\phi\phi}}{\partial t} - \frac{2r\omega}{h}A_{\phi z}\right) = 0 \tag{6.27g}$$

$$A_{\phi z} + \tau \left(\frac{\partial A_{\phi z}}{\partial t} - \frac{r\omega}{h} A_{zz} \right) = \frac{\tau r \omega}{h} \tag{6.27h}$$

$$A_{zz} + \tau \frac{\partial A_{zz}}{\partial t} = 0\,. \tag{6.27i}$$

If we neglect the term $\frac{\mathrm{d}\omega}{\mathrm{d}t}$ according to the above-discussed assumption and take the initial conditions (6.2) into account, then the equations have the solution

$$p = G \left(\frac{\tau\omega}{h} \right)^2 \left(R^2 - r^2 \right) \left(1 - (1 + \frac{t}{\tau}) e^{-t/\tau} \right) \tag{6.28}$$

$$A_{rr} = A_{r\phi} = A_{rz} = A_{zz} = 0 \tag{6.29}$$

$$A_{\phi\phi} = 2 \left(\frac{\tau r \omega}{h} \right)^2 \left(1 - (1 + \frac{t}{\tau}) e^{-t/\tau} \right) \tag{6.30}$$

$$A_{\phi z} = \frac{\tau r \omega}{h} \left(1 - e^{-t/\tau} \right)\,. \tag{6.31}$$

The torque integrated according to (6.4) is

$$M = \frac{\pi \omega R^4}{2h} \left(\eta + \tau G \left(1 - e^{-t/\tau} \right) \right)\,. \tag{6.32}$$

We see that the torque consists of two parts; the first one, which is due to viscosity, is constant and the second one, which corresponds to elastic behavior, relaxes to a constant value. It is therefore clearly evident that the Oldroyd-B model is not capable of capturing the overshoots in torque, which have been observed in the experiments (see Figure 1.2); however, it is still reasonable to try fitting the experimental data with this formula, which we will proceed to in Section 6.4.

6.3.2 Model 1

We proceed similarly as in the case of Oldroyd-B model.

Steady flow

Substituting the ansatz

$$p = p(r,z), \quad \mathbf{v} = \frac{\omega r z}{h} \mathbf{e}_\phi, \quad b = b(r,z) \tag{6.33}$$

$$\mathbf{B}^\delta_{\kappa_p} = \begin{pmatrix} B^\delta_{rr}(r,z) & B^\delta_{r\phi}(r,z) & B^\delta_{rz}(r,z) \\ B^\delta_{r\phi}(r,z) & B^\delta_{\phi\phi}(r,z) & B^\delta_{\phi z}(r,z) \\ B^\delta_{rz}(r,z) & B^\delta_{\phi z}(r,z) & -B^\delta_{rr}(r,z) - B^\delta_{\phi\phi}(r,z) \end{pmatrix} \tag{6.34}$$

into the governing equations of Model 1 (2.44) and neglecting the convective term, we obtain

$$0 = -\frac{\partial p}{\partial r} + \mu\left(\frac{\partial B^{\delta}_{rr}}{\partial r} + \frac{B^{\delta}_{rr}}{r} - \frac{B^{\delta}_{\phi\phi}}{r} + \frac{\partial B^{\delta}_{rz}}{\partial z}\right) \tag{6.35a}$$

$$0 = \mu\left(\frac{\partial B^{\delta}_{r\phi}}{\partial r} + \frac{2B^{\delta}_{r\phi}}{r} + \frac{\partial B^{\delta}_{\phi z}}{\partial z}\right) \tag{6.35b}$$

$$0 = -\frac{\partial p}{\partial z} + \mu\left(\frac{\partial B^{\delta}_{rz}}{\partial r} + \frac{B^{\delta}_{rz}}{r} - \frac{\partial B^{\delta}_{rr}}{\partial z} - \frac{\partial B^{\delta}_{\phi\phi}}{\partial z}\right) \tag{6.35c}$$

$$\mu B^{\delta}_{rr} = -\frac{\epsilon_1 r\omega}{3h} B^{\delta}_{\phi z} \tag{6.35d}$$

$$\mu B^{\delta}_{r\phi} = \frac{\epsilon_1 r\omega}{2h} B^{\delta}_{rz} \tag{6.35e}$$

$$\mu B^{\delta}_{rz} = 0 \tag{6.35f}$$

$$\mu B^{\delta}_{\phi\phi} = \frac{2\epsilon_1 r\omega}{3h} B^{\delta}_{\phi z} \tag{6.35g}$$

$$\mu B^{\delta}_{\phi z} = \epsilon_1\left(-\frac{r\omega}{2h} B^{\delta}_{rr} - \frac{r\omega}{2h} B^{\delta}_{\phi\phi} + \frac{r\omega}{6h} b\right) \tag{6.35h}$$

$$1 = \det\left(\mathbf{B}^{\delta}_{\kappa_p} + \frac{1}{3} b\mathbf{I}\right). \tag{6.35i}$$

These equations can be solved in the following way. From (6.35e) and (6.35f) follows that

$$B^{\delta}_{r\phi} = B^{\delta}_{rz} = 0\,, \tag{6.36}$$

the incompressibility constraint (6.35i) then simplifies to

$$1 = \left(B^{\delta}_{rr} + \frac{b}{3}\right)\left[\left(B^{\delta}_{\phi\phi} + \frac{b}{3}\right)\left(-B^{\delta}_{rr} - B^{\delta}_{\phi\phi} + \frac{b}{3}\right) - {B^{\delta}_{\phi z}}^{2}\right]. \tag{6.37}$$

The remaining components of $\mathbf{B}^{\delta}_{\kappa_p}$ and b can be expressed from (6.35d), (6.35g) and (6.35h) using $B^{\delta}_{\phi z}$ as

$$B^{\delta}_{rr} = -\frac{2ar}{3} B^{\delta}_{\phi z} \tag{6.38}$$

$$B^{\delta}_{\phi\phi} = \frac{4ar}{3} B^{\delta}_{\phi z} \tag{6.39}$$

$$b = \left(2ar + \frac{3}{ar}\right) B^{\delta}_{\phi z}\,, \tag{6.40}$$

where for the simplicity of the notation we have defined

$$a := \frac{\epsilon_1}{2\mu}\frac{\omega}{h}\,. \tag{6.41}$$

Now, substituting these results into (6.37) yields a cubic equation for $B^{\delta}_{\phi z}$, the only real solution of which is

$$B^{\delta}_{\phi z} = \frac{ar}{\sqrt[3]{1+a^2r^2}}\,. \tag{6.42}$$

Thus, we have solutions for all the components of $\mathbf{B}_{\kappa_p}$ and b. Using these results, the momentum equations (6.35a) – (6.35c) simplify to

$$\frac{\partial p}{\partial r} = \mu\left(\frac{\partial B^{\delta}_{rr}}{\partial r} + \frac{3B^{\delta}_{rr}}{r}\right) \tag{6.43}$$

$$\frac{\partial p}{\partial z} = 0\,. \tag{6.44}$$

Since the right-hand side of (6.43) does not depend on z, the integrability condition for pressure is satisfied and the pressure can be expressed as

$$p = \mu\left(B^{\delta}_{rr} + \int \frac{3B^{\delta}_{rr}}{r}\,\mathrm{d}r\right) = \frac{3\mu}{2}\left(1+a^2r^2\right)^{2/3} - \frac{\mu}{6}\frac{9+13a^2r^2}{\sqrt[3]{1+a^2r^2}}\,. \tag{6.45}$$

Again, our solution satisfies the boundary conditions (6.1). The torque integrated according to (6.4) is

$$M = \frac{\pi\epsilon_0\omega R^4}{4h} + \frac{3\pi\mu}{10a^3}\left[\left(1+a^2R^2\right)^{2/3}\left(2a^2R^2-3\right)+3\right]\,. \tag{6.46}$$

Unsteady flow

Upon substituting the ansatz

$$p = p(t,r,z), \quad \mathbf{v} = \frac{\omega(t)rz}{h}\mathbf{e}_{\phi}, \quad b = b(t,r,z) \tag{6.47}$$

$$\mathbf{B}^{\delta}_{\kappa_p} = \begin{pmatrix} B^{\delta}_{rr}(t,r,z) & B^{\delta}_{r\phi}(t,r,z) & B^{\delta}_{rz}(t,r,z) \\ B^{\delta}_{r\phi}(t,r,z) & B^{\delta}_{\phi\phi}(t,r,z) & B^{\delta}_{\phi z}(t,r,z) \\ B^{\delta}_{rz}(t,r,z) & B^{\delta}_{\phi z}(t,r,z) & -B^{\delta}_{rr}(t,r,z) - B^{\delta}_{\phi\phi}(t,r,z) \end{pmatrix} \tag{6.48}$$

into the governing equations of Model 1 (2.44) we get

$$0 = -\frac{\partial p}{\partial r} + \mu\left(\frac{\partial B^{\delta}_{rr}}{\partial r} + \frac{B^{\delta}_{rr}}{r} - \frac{B^{\delta}_{\phi\phi}}{r} + \frac{\partial B^{\delta}_{rz}}{\partial z}\right) \tag{6.49a}$$

$$\rho\frac{rz}{h}\frac{\mathrm{d}\omega}{\mathrm{d}t} = \mu\left(\frac{\partial B^{\delta}_{r\phi}}{\partial r} + \frac{2B^{\delta}_{r\phi}}{r} + \frac{\partial B^{\delta}_{\phi z}}{\partial z}\right) \tag{6.49b}$$

$$0 = -\frac{\partial p}{\partial z} + \mu\left(\frac{\partial B^{\delta}_{rz}}{\partial r} + \frac{B^{\delta}_{rz}}{r} - \frac{\partial B^{\delta}_{rr}}{\partial z} - \frac{\partial B^{\delta}_{\phi\phi}}{\partial z}\right) \tag{6.49c}$$

$$\mu B^{\delta}_{rr} = \epsilon_1 \left(-\frac{1}{2}\frac{\partial B^{\delta}_{rr}}{\partial t} - \frac{r\omega}{3h} B^{\delta}_{\phi z} \right) \tag{6.49d}$$

$$\mu B^{\delta}_{r\phi} = \epsilon_1 \left(-\frac{1}{2}\frac{\partial B^{\delta}_{r\phi}}{\partial t} + \frac{r\omega}{2h} B^{\delta}_{rz} \right) \tag{6.49e}$$

$$\mu B^{\delta}_{rz} = -\frac{\epsilon_1}{2}\frac{\partial B^{\delta}_{rz}}{\partial t} \tag{6.49f}$$

$$\mu B^{\delta}_{\phi\phi} = \epsilon_1 \left(-\frac{1}{2}\frac{\partial B^{\delta}_{\phi\phi}}{\partial t} + \frac{2r\omega}{3h} B^{\delta}_{\phi z} \right) \tag{6.49g}$$

$$\mu B^{\delta}_{\phi z} = \epsilon_1 \left(-\frac{1}{2}\frac{\partial B^{\delta}_{\phi z}}{\partial t} - \frac{r\omega}{2h} B^{\delta}_{rr} - \frac{r\omega}{2h} B^{\delta}_{\phi\phi} + \frac{r\omega}{6h} b \right) \tag{6.49h}$$

$$1 = \det\left(\mathbf{B}^{\delta}_{\kappa_p} + \frac{1}{3} b \mathbf{I} \right) . \tag{6.49i}$$

Although these equations do not have an analytical solution, they can still be noticeably simplified in the following way. Firstly, as in the steady state, equations (6.49e) – (6.49f) have together with the initial condition (6.2c) the solution

$$B^{\delta}_{r\phi} = B^{\delta}_{rz} = 0 . \tag{6.50}$$

Next, upon multiplying equation (6.49d) by 2 and adding it to (6.49g) we arrive at

$$\mu(2B^{\delta}_{rr} + B^{\delta}_{\phi\phi}) = \epsilon_1 \frac{\partial}{\partial t}(2B^{\delta}_{rr} + B^{\delta}_{\phi\phi}), \tag{6.51}$$

which together with the initial condition (6.2c) yields

$$B^{\delta}_{\phi\phi} = -2B^{\delta}_{rr} . \tag{6.52}$$

Furthermore, we observe that none of the initial conditions as well as none of the equations (6.49d) – (6.49i) depends on z and therefore also the components of $\mathbf{B}^{\delta}_{\kappa_p}$ and b do not depend on this coordinate. In view of these results equations (6.49) simplify to

$$\frac{\partial p}{\partial r} = \mu \left(\frac{\partial B^{\delta}_{rr}}{\partial r} - \frac{B^{\delta}_{rr}}{r} \right) \tag{6.53a}$$

$$\frac{\partial p}{\partial z} = 0 \tag{6.53b}$$

$$\mu B^{\delta}_{rr} = \epsilon_1 \left(-\frac{1}{2}\frac{\partial B^{\delta}_{rr}}{\partial t} - \frac{r\omega}{3h} B^{\delta}_{\phi z} \right) \tag{6.53c}$$

$$\mu B^{\delta}_{\phi z} = \epsilon_1 \left(-\frac{1}{2}\frac{\partial B^{\delta}_{\phi z}}{\partial t} + \frac{r\omega}{2h} B^{\delta}_{rr} + \frac{r\omega}{6h} b \right) \tag{6.53d}$$

$$1 = \left(B^{\delta}_{rr} + \frac{b}{3}\right)\left[\left(-2B^{\delta}_{rr} + \frac{b}{3}\right)\left(B^{\delta}_{rr} + \frac{b}{3}\right) - {B^{\delta}_{\phi z}}^{2}\right]. \tag{6.53e}$$

We observe again that the integrability condition for pressure is satisfied. Since we are interested only in $B^{\delta}_{\phi z}$, we need to solve only the last three equations. Unfortunately, these equations cannot be solved analytically but only numerically. In order to accomplish this, we rewrite them in the weak form

$$\int_0^R \frac{\epsilon_1}{2}\frac{\partial B^{\delta}_{rr}}{\partial t} r W_{rr}\,\mathrm{d}r = \int_0^R \left(-\mu B^{\delta}_{rr} - \frac{\epsilon_1 r\omega}{3h} B^{\delta}_{\phi z}\right) r W_{rr}\,\mathrm{d}r \tag{6.54a}$$

$$\int_0^R \frac{\epsilon_1}{2}\frac{\partial B^{\delta}_{\phi z}}{\partial t} r W_{r\phi}\,\mathrm{d}r = \int_0^R \left(-\mu B^{\delta}_{\phi z} + \frac{\epsilon_1 r\omega}{2h} B^{\delta}_{rr} + \frac{\epsilon_1 r\omega}{6h} b\right) r W_{r\phi}\,\mathrm{d}r \tag{6.54b}$$

$$0 = \int_0^R \left\{\left(B^{\delta}_{rr} + \frac{b}{3}\right)\left[\left(-2B^{\delta}_{rr} + \frac{b}{3}\right)\left(B^{\delta}_{rr} + \frac{b}{3}\right) - {B^{\delta}_{\phi z}}^{2}\right] - 1\right\} r w\,\mathrm{d}r\,. \tag{6.54c}$$

6.4 Comparison with experimental data

In this section we compare the above obtained results with the experimental data. We will proceed in the following way. Firstly, we fit the data with the analytical formula (6.32) for Oldroyd-B using the least squares method. For this purpose, we employ the `MATLAB` function `fit`. This delivers some values of the material moduli η, μ and τ. Next, we recalculate the corresponding values of material parameters ϵ_0, ϵ_1 and μ using (2.52). Finally, we use them as initial values for minimizing the L^2 norm of the difference between the experimental curves and the curves obtained by solving equations (6.54) with the aid of `MATLAB` function `fminsearch`.

The results of this procedure are shown in Figures 6.3 and 6.4. Each of the experimental curves has been fitted separately, even though the material moduli at the same temperature should be equal. The values of material moduli of both models are summarized in Table 6.1.

It is clearly evident that Oldroyd-B is not capable of capturing any overshoots at all. Unfortunately, Model 1 does not fit the experimental data any better than Oldroyd-B, even though it can in principle exhibit overshoots in torque for certain values of parameters. Also the material moduli obtained by fitting the data by means of Model 1 are very close to those obtained by Oldroyd-B (after recalculating using (2.52)). We therefore conclude that under the conditions corresponding to the experiment both models coincide and thus the observed overshoots in torque cannot be explained merely by the fact that the elastic part of the deformation is large.

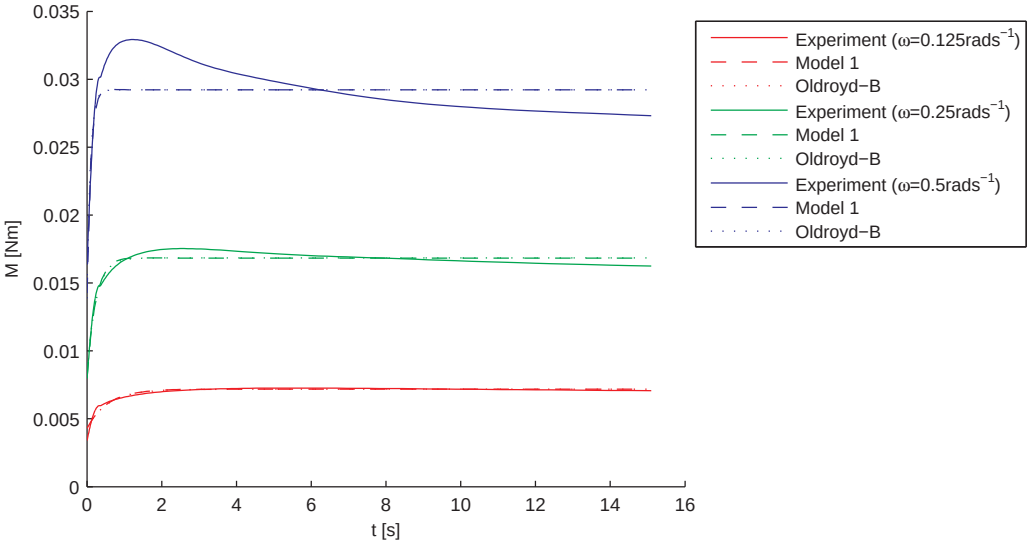

Figure 6.3: Torque at $\theta = 25\,^{\circ}\mathrm{C}$ fitted with Oldroyd-B and Model 1.

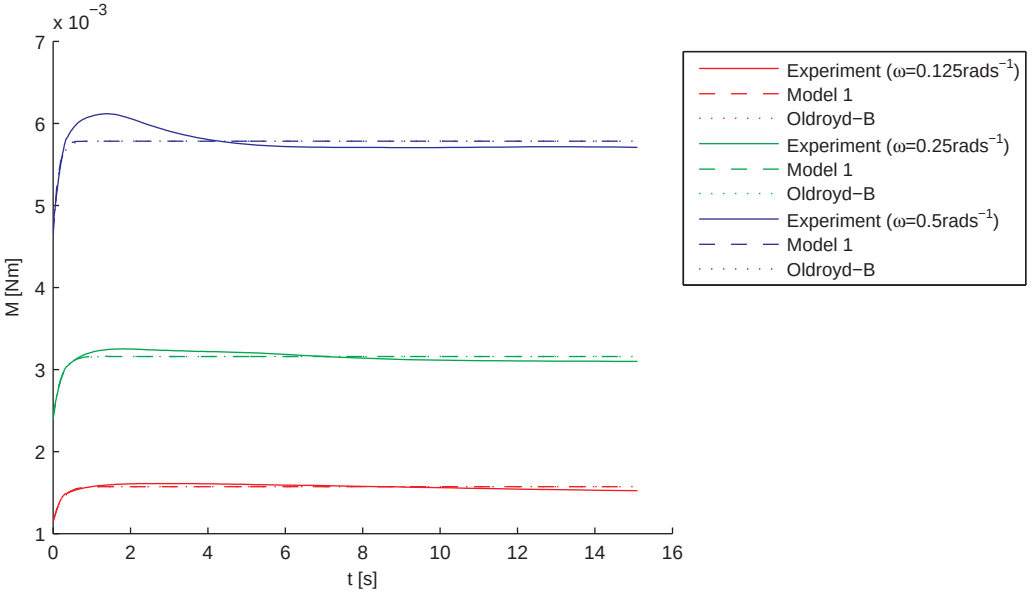

Figure 6.4: Torque at $\theta = 35\,^{\circ}\mathrm{C}$ fitted by Oldroyd-B and Model 1.

	θ	25 °C			35 °C		
	$\frac{\omega}{\text{rad.s}^{-1}}$	0.125	0.25	0.5	0.125	0.25	0.5
Oldroyd-B	$\frac{\eta}{10^3\,\text{Pa.s}}$	86	82	69	23	24	23
	$\frac{G}{10^3\,\text{Pa}}$	99	360	840	34	40	40
	$\frac{\tau}{\text{s}}$	0.57	0.24	0.09	0.24	0.19	0.14
Model 1	$\frac{\epsilon_0}{10^3\,\text{Pa.s}}$	170	160	140	46	48	46
	$\frac{\epsilon_1}{10^3\,\text{Pa.s}}$	120	180	150	17	15	11
	$\frac{\mu}{10^3\,\text{Pa}}$	100	370	760	36	38	42

Table 6.1: Estimate of material moduli obtained by fitting the data by Oldroyd-B and Model 1.

6.5 Solution without simplifications

Now, let us proceed to the solution of the flow without any simplifications. Our aim will be firstly to confirm the results obtained in the previous section and secondly to investigate the behavior of the secondary flow.

6.5.1 Weak formulation

In this section we reformulate the problem described in Section 6.1 from the 3D cylinder Ω to the 2D-cross section Σ. The boundary conditions on $\partial\Omega$ imply the following boundary conditions on $\partial\Sigma$:

$$\mathbf{Te}_r = 0 \text{ on } \gamma_1 \tag{6.55}$$

$$v_r = v_z = 0, v_\phi = \omega r \text{ on } \gamma_2 \tag{6.56}$$

$$\mathbf{v} = 0 \text{ on } \gamma_4 \tag{6.57}$$

The conditions on the axis of symmetry deserve special attention. If we formally define negative r coordinates by

$$\mathbf{v}(-r, \phi, z) := \mathbf{v}(r, \phi + \pi, z)\,, \tag{6.58}$$

the conditions implied by the symmetry for the components of velocity may be written in the form

$$v_r(-r, z) = -v_r(r, z) \tag{6.59}$$

$$v_\phi(-r, z) = -v_\phi(r, z) \tag{6.60}$$

$$v_z(-r, z) = v_z(r, z)\,. \tag{6.61}$$

Setting $r = 0$ in the first and the second equation delivers the following two conditions of Dirichlet type

$$v_r(0, z) = 0 \tag{6.62}$$
$$v_\phi(0, z) = 0\,, \tag{6.63}$$

which must be taken into account by appropriate choice of the spaces in the weak formulation while the remaining third condition of Neumann type

$$T_{rz} = 0 \tag{6.64}$$

will be embedded in the variational equations of the problem.

Now let us show how the weak formulation of the equations (3.1) and (3.2) can be under the assumption of axial symmetry transformed from the 3D domain Ω to the 2D cross-section Σ. We will demonstrate it in the case of Oldroyd-B, the procedure for Model 1 is completely analogous.

To accomplish this we write all the integrals over Ω occurring in (3.1) in cylindrical coordinates, factor the terms not depending on ϕ out of the integral over ϕ and finally rewrite the result as an integral over the cross-section Σ. For (3.1a) the procedure looks as follows

$$\begin{aligned} 0 = \int_\Omega \operatorname{div} \mathbf{v} q \,\mathrm{d}\mathbf{x} = \\ = \int_0^R \mathrm{d}r \int_0^h \mathrm{d}z \int_0^{2\pi} \mathrm{d}\phi \;\operatorname{div} \mathbf{v} r q = \int_0^R \mathrm{d}r \int_0^h \mathrm{d}z \;\operatorname{div} \mathbf{v} r \left(\int_0^{2\pi} q \,\mathrm{d}\phi \right) = \\ = \int_0^R \mathrm{d}r \int_0^h \mathrm{d}z \operatorname{div} \mathbf{v} r \hat{q} = \int_\Sigma \operatorname{div} \mathbf{v} r \hat{q} \,\mathrm{d}\Sigma\,. \end{aligned} \tag{6.65}$$

Here we have defined a new '2D' test function $\hat{q}$ using the old '3D' test function q through the relation

$$\hat{q}(r, z) = \int_0^{2\pi} q(r, \phi, z) \,\mathrm{d}\phi\,, \tag{6.66}$$

the variable r in the last integrand of (6.65) emerges from the Jacobian of the cylindrical coordinates. Exactly the same procedure applied to (3.1b) and (3.1c) delivers

$$\int_\Sigma \rho \dot{\mathbf{v}} \cdot \hat{\mathbf{u}} r \,\mathrm{d}\Sigma = -\int_\Sigma \mathbf{T} \cdot \nabla \hat{\mathbf{u}} r \,\mathrm{d}\Sigma \tag{6.67}$$
$$\int_\Sigma (\mathbf{A} + \tau \overset{\nabla}{\mathbf{A}}) \cdot \hat{\mathbf{S}} r \,\mathrm{d}\Sigma = \int_\Sigma 2\tau \mathbf{D} \cdot \hat{\mathbf{S}} r \,\mathrm{d}\Sigma\,, \tag{6.68}$$

where we have defined the '2D' test functions

$$\hat{\mathbf{u}}(r,z) = \int_0^{2\pi} \mathbf{u}(r,\phi,z)\,\mathrm{d}\phi \tag{6.69}$$

$$\hat{\mathbf{S}}(r,z) = \int_0^{2\pi} \mathbf{S}(r,\phi,z)\,\mathrm{d}\phi\,. \tag{6.70}$$

Thus, the problem describing the axially symmetric flow of an Oldroyd-B fluid in the cylinder may be formulated as follows

Find $(p,\mathbf{v},\mathbf{A}) : \langle 0,T\rangle \to \hat{Q}\times\hat{V}\times\hat{S}$ *such that*

$$\int_\Sigma (\operatorname{div}\mathbf{v})\hat{q}r\,\mathrm{d}\Sigma = 0 \tag{6.71a}$$

$$\int_\Sigma \rho\dot{\mathbf{v}}\cdot\hat{\mathbf{u}}r\,\mathrm{d}\Sigma = -\int_\Sigma \mathbf{T}\cdot\nabla\hat{\mathbf{u}}r\,\mathrm{d}\Sigma \tag{6.71b}$$

$$\int_\Sigma (\mathbf{A}+\tau\overset{\triangledown}{\mathbf{A}})\cdot\hat{\mathbf{S}}r\,\mathrm{d}\Sigma = \int_\Sigma 2\tau\mathbf{D}\cdot\hat{\mathbf{S}}r\,\mathrm{d}\Sigma \tag{6.71c}$$

for all $\hat{q}\in\hat{Q}$, $\hat{\mathbf{u}}\in\hat{V}_0$ *and* $\hat{\mathbf{A}}\in\hat{S}_0$.

Analogously, the weak formulation of the problem describing the axially symmetric flow of Model 1 in the cylinder is

Find $(p,\mathbf{v},\mathbf{B}^\delta_{\kappa_p},b) : \langle 0,T\rangle \to \hat{Q}\times\hat{V}\times\hat{W}\times\hat{B}$ *such that*

$$0 = \int_\Sigma (\operatorname{div}\mathbf{v})\hat{q}r\,\mathrm{d}\Sigma \tag{6.72a}$$

$$\int_\Sigma \varrho\dot{\mathbf{v}}\cdot\hat{\mathbf{u}}r\,\mathrm{d}\Sigma = -\int_\Sigma \mathbf{T}\cdot\nabla\hat{\mathbf{u}}r\,\mathrm{d}\Sigma \tag{6.72b}$$

$$\int_\Sigma \mu\mathbf{B}^\delta_{\kappa_p}\cdot\hat{\mathbf{S}}r\,\mathrm{d}\Sigma = \epsilon_1\int_\Sigma\left(-\frac{1}{2}\overset{\triangledown}{\mathbf{B}}{}^\delta_{\kappa_p}+\frac{1}{3}b\mathbf{D}-\frac{1}{3}(\mathbf{D}\cdot\mathbf{B}^\delta_{\kappa_p})\mathbf{I}\right)\cdot\hat{\mathbf{S}}r\,\mathrm{d}\Sigma \tag{6.72c}$$

$$0 = \int_\Sigma\left[\det\left(\mathbf{B}^\delta_{\kappa_p}+\frac{1}{3}b\mathbf{I}\right)-1\right]\hat{w}r\,\mathrm{d}\Sigma \tag{6.72d}$$

for all $\hat{q}\in\hat{Q}$, $\hat{\mathbf{u}}\in\hat{V}_0$, $\hat{\mathbf{S}}\in\hat{S}_0$ *and* $\hat{w}\in\hat{B}_0$.

6.5.2 Numerical results

The above presented weak formulations of the governing equations were discretised using Galerkin method. The chosen shape functions were the same as in planar 2D case, i.e. discontinuous piecewise linear functions for pressure and continuous piecewise quadratic functions for all other variables, the corresponding mesh is shown in Figure 6.5. Note that to rewrite the weak equations (6.71) or (6.72) into the cylindrical coordinates is rather a hard

work, because e.g. the equations for Model 1 in cylindrical coordinates have altogether 116 terms. To avoid errors, we have developed a special package for Maple, which converts the equations in tensorial form into arbitrary orthogonal curvilinear coordinates and then exports them to Comsol.

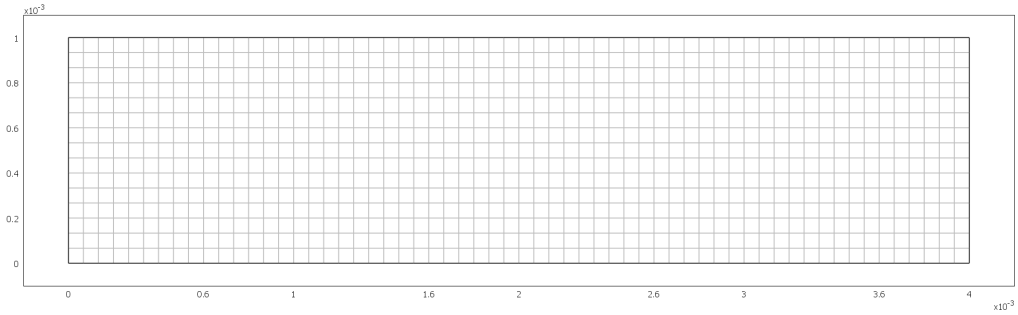

Figure 6.5: The most refined mesh (900 elements).

The numerical tests have been conducted for both Oldroyd-B and Model 1 in both steady and unsteady case without any simplifications. In the steady case we have obtained solutions for various values of material moduli and these correspond well to the analytical solutions presented in Section 6.3. The secondary flow is of the order of magnitude $10^{-14}\,\mathrm{m.s}^{-1}$ and does not have any measurable influence on the result.

In the unsteady case we have investigated stress relaxation in both models. The results are quite analogous to the parallel plate flow. On the upper plate we prescribed the following Dirichlet condition

$$\mathbf{v} = \omega_0 r H_S(t)\mathbf{e}_\phi, \quad \omega_0 = \mathrm{const}\,. \tag{6.73}$$

where $H_S(t)$ is the step function smoothened over a finite interval of length S. If this interval was shorter than the characteristic time (6.14), say $10^{-13}\,\mathrm{s}$ and the time step was correspondingly fine, we were able to study the transient effect during which the steady velocity profile establishes. The development of this profile is shown in Figure 6.6. If the step function was smoothened over an interval longer than the characteristic time (6.14), say $10^{-4}\,\mathrm{s}$, the velocity was equal to that in the steady case throughout the whole simulation.

We have checked that the solutions to the unsteady problems converge to the analytical steady state solutions and that they are equal to the approximate solutions obtained in Section 6.3. Moreover, we have checked that the results are independent of mesh and time step size.

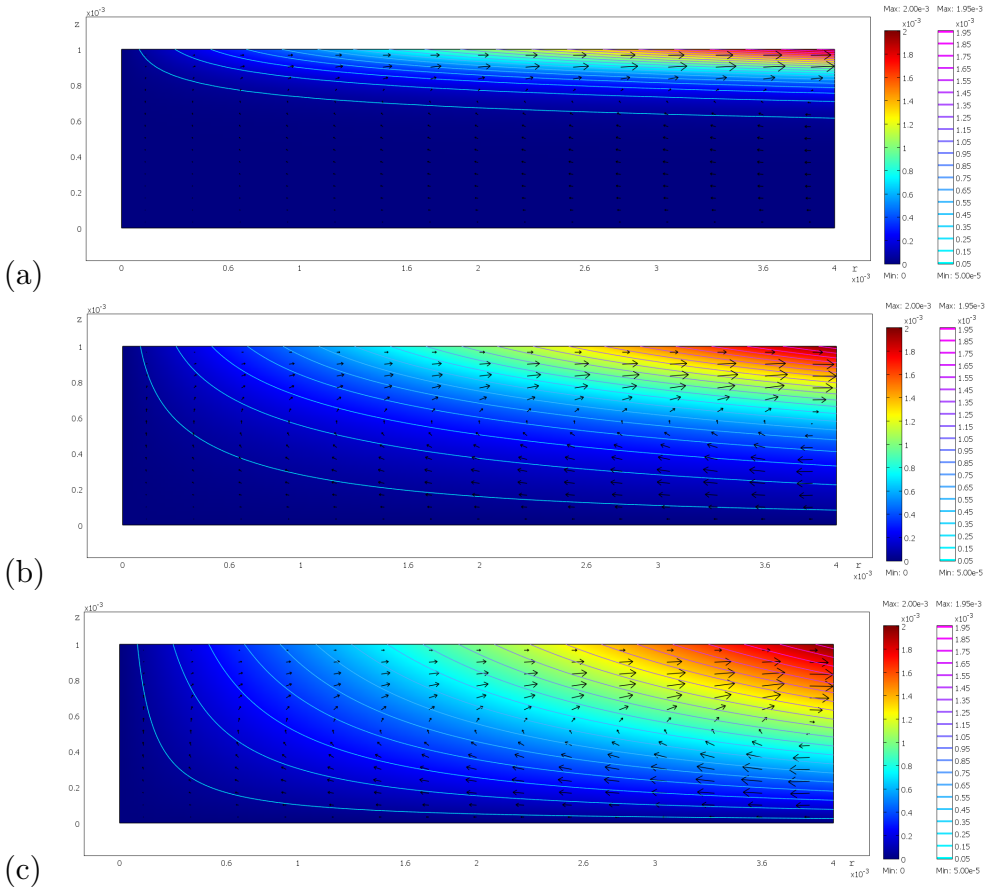

Figure 6.6: The velocity profile for Oldroyd-B in the rz cross-section at time (a) $t = 10^{-10}$ s, (b) $t = 10^{-9}$ s, (c) $t = 10^{-8}$ s after triggering the experiment. The values of material constants are $\eta = 8.10^4$ Pa.s, $\mu = 4.10^5$ Pa, $\tau = 1$ s. The velocity profile (c) is equal to that in the steady state. The results for Model 1 are the same.

Conclusions

In this thesis we have been concerned with numerical simulations of flows of viscoelastic fluids applicable to complicated materials as asphalt. We deal with two models, which are presented in Chapter 2, namely the Oldroyd-B and a more general nonlinear model denoted as Model 1 and investigate both steady and unsteady flows of fluids governed by these models at three different geometries.

First, we consider flow between two parallel plates. We are able to find analytical solutions for both models in the steady case and also for stress relaxation of the Oldroyd-B fluid. The stress relaxation in the case of Model 1 has to be solved numerically.

Secondly, we investigate the flow of an Oldroyd-B fluid in a 4:1 planar contraction, which is a standard benchmark in the area of numerical simulations of flows of viscoelastic fluids. This benchmark is a difficult one because of the occurrence of the stress singularity at the re-entrant corner. To avoid spurious oscillations in the solution, we have to stabilize the equations using streamline diffusion method. We compare our solution with results in the literature finding out, that our results are well comparable for $\mathrm{We} \leq 1$ when $\mathrm{Re} = 0$ and for $\mathrm{We} \leq 1.5$ when $\mathrm{Re} = 1$. For greater values of We a significant departure from the results published in the literature is observed, which is very likely due to quite a large amount of artificial diffusion added to the equations in order that we are able to solve them. In addition, there is still not a fair agreement on the correct results for this benchmark among different authors and from this point of view our results are acceptable.

The last problem we deal with is axially symmetric flow inside a cylinder. Neglecting the convective term, we find analytical solution in the steady state. If we neglect the whole material time derivative of the velocity, we find approximate solution for shear stress relaxation of an Oldroyd-B fluid and simplify the equations for Model 1 to a set of partial differential equations in one spatial variable and solve them numerically. Besides that, we solve the full equations for both models numerically without any simplifications, the results of this full simulation being in a good agreement with the simplified solutions.

Finally, we fit the experimental data concerning steady shear rate experiment for asphalt performed by Dr. J. Murali Krishnan with both considered models. Oldroyd-B fits the data quite well, but it is not capable of capturing the overshoots in torque which have been observed in the experiment. A disappointing result is, that Model 1 does not fit the data any better than Oldroyd-B, even though it can exhibit overshoots in torque for some values of material moduli and boundary conditions. Since the difference between these two models is, that Model 1 considers large elastic deformations while Oldroyd-B does not, we conclude, that in this experiment the measured overshoots in torque are not caused by the fact, that the elastic deformations are large.

Further work should be focused on investigating other models for viscoelastic fluids such as Burgers model and its generalizations. When a better agreement with present experimental data is found for a certain model, it should be further tested in other experimental situations. We believe, that the methods presented in this thesis are well applicable to other models and geometries.

Bibliography

[1] Internet http://www.physics.uq.edu.au/pitchdrop/pitchdrop.shtml. 2

[2] *Comsol Multiphysics User's guide*. COMSOL AB, 2006. 16

[3] Málek J. and Rajagopal K. R. Incompressible rate type fluids with pressure and shear–rate dependent material moduli. *Nonlinear Analysis: Real World Applications*, 8(1):156–164, 2007. 10

[4] Wilson J. H. *Lecture notes on polymeric fluids*. 2006. Lecture notes in electronic form available at http://www.ucl.ac.uk/˜ucahhwi/GM05/. 7

[5] Krishnan J. M. personal communication. 2006-2007. 2, 4

[6] Krishnan J. M. and Rajagopal K. R. Review of the uses and modeling of bitumen from ancient to modern times. *Applied Mechanics Reviews*, 56(2):149–214, 2003. 1

[7] Krishnan J. M. and Rajagopal K. R. On the mechanical behavior of asphalt. *Mechanics of Materials*, 11(37):1085–1100, 2005. 1

[8] Rajagopal K. R. and Srinivasa A. R. Mechanics of the inelastic behavior of materials - part 2, inelastic response. *International Journal of Plasticity*, 14(10-11):969–995, 1998. 7

[9] Rajagopal K. R. and Srinivasa A. R. Mechanics of the inelastic behavior of materials part 1, theoretical underpinnings. *International Journal of Plasticity*, 14(10-11):945–967, 1998. 7

[10] Rajagopal K. R. and Srinivasa A. R. A thermodynamic frame work for rate type fluid models. *Journal of Non-Newtonian Fluid Mechanics*, 88(3):207–227, 2000. 7

[11] Rajagopal K. R. and Srinivasa A. R. On the thermomechanics of materials that have multiple natural configurations part i: Viscoelasticity and classical plasticity. *Zeitschrift für Angewandte Mathematik und Physik*, 55(5):861–893, 2004. 8

[12] Rajagopal K. R. and Srinivasa A. R. On thermomechanical restrictions of continua. *Proc. R. Soc. London A Mat.*, 460:1074–1093, 2004. 10

[13] Le Tallec P. *Numerical analysis of viscoelastic problems*. Springer Verlag, 1990. 15

[14] Kundu P. K. and Cohen I. R. *Fluid mechanics*. Academic Press, 2002. 17

[15] Owens R. G. and Phillips T. N. *Computational Rheology*. Imperial College Press, 2002. 14, 15, 16

[16] Davis T. A. and Duff I. S. An unsymmetric-pattern multifrontal method for sparse LU factorization. *SIAM Journal on Matrix Analysis and Applications*, 18(1):140–158, 1997. 16

[17] Davis T. A. and Duff I. S. A combined unifrontal/multifrontal method for unsymmetric sparse matrices. *ACM Transactions on Mathematical Software*, 25(1):1–19, 1999. 16

[18] Phillips T. N. and Williams A. J. Viscoelastic flow through a planar contraction using a semi-Lagrangian finite volume method. *Journal of Non-Newtonian Fluid Mechanics*, 87:215–246, 1999. 29, 30, 32, 33, 34, 35, 36

[19] Martinec Z. *Continuum Mechanics*. 2003. Lecture notes in electronic form available at http://geo.mff.cuni.cz/teaching_cz.htm. 5